Bulletin of the Geological Survey of Japan, vol. 74 (1), p. 1–40, 2023

Article

Geology and accretionary age of the Otori Unit, North Kitakami Belt

MUTO Shun[1,*], ITO Tsuyoshi[1] and MURAYAMA Masafumi[2, 3]

MUTO Shun, ITO Tsuyoshi and MURAYAMA Masafumi (2023) Geology and accretionary age of the Otori Unit, North Kitakami Belt. *Bulletin of the Geological Survey of Japan*, vol. 74(1), p. 1–40, 13 figs, 2 tables, 5 plates and 3 appendices.

Abstract: The North Kitakami Belt in Northeast Japan mainly comprises accretionary complexes formed during the Jurassic to earliest Cretaceous. The accretionary complex of the North Kitakami Belt is less studied compared to the age-equivalent accretionary complexes in Southwest Japan. Here, we provide additional data on the accretionary complex formerly classified as the Otori Unit, distributed in the northeastern part of the North Kitakami Belt in the upper reaches of the Akka River in Iwate Prefecture. Based on detailed field mapping, we clarified that the Otori Unit is composed of the structurally lower coherent facies of chert and siliceous mudstone (Okoshizawa Subunit) and the structurally upper mixed facies of mudstone, sandstone, chert and minor basaltic rocks (Osakamoto Subunit). Manganese nodules from siliceous mudstone within the Okoshizawa Subunit yielded radiolarians indicating the Bathonian (upper Middle Jurassic). Detrital zircon grains from sandstone in the Osakamoto Subunit has a youngest age of ~170 Ma (YC1σ: 171.8 ± 2.4 Ma; YSG: 170.9 ± 3.8 Ma). Based on the radiolarian and detrital zircon ages, the accretionary age of the Otori Unit is estimated as the Bathonian. Our new data were also considered to discuss the correlation between the North Kitakami Belt and the Southern Chichibu Belt in Southwest Japan. The Otori Unit corresponds to the Ohirayama Unit of the Southern Chichibu Belt in structural position, and the two units are similar in being a mixed facies and have overlapping accretionary age. However, the Otori Unit lacks limestone and has a considerably younger age for siliceous mudstone, suggesting that the two units may not be strictly correlative.

Keywords: Akka River, Bathonian, conodont, detrital zircon, Jurassic accretionary complex, North Kitakami Belt, radiolarian

1. Introduction

The North Kitakami Belt in Northeast Japan mainly consists of an accretionary complex that was formed during the Jurassic to earliest Cretaceous (the term "Jurassic accretionary complex" is used hereafter) (Ehiro *et al.*, 2005; Kojima *et al.*, 2016). The accretionary complex of the North Kitakami Belt was at first regarded as deep-sea facies deposited during the Paleozoic based on fossils in limestone (Minato, 1950; Onuki, 1956; Yoshida and Katada, 1964). Following the finding of Mesozoic fossils from the eastern part of the northern Kitakami Mountains, the term "North Kitakami Belt" was used by some researchers to refer to the western "Paleozoic" part (e.g., Shimazu *et al.*, 1970). It was assumed that the age of strata becomes younger towards the east, due to migration of the depocentre from west to east (Sugimoto, 1969, 1974, 1980; Yamaguchi *et al.*, 1979; Yamaguchi, 1981). However, Triassic conodonts discovered from throughout the northern Kitakami Mountains showed that the then adopted geological model was no longer plausible (Toyohara *et al.*, 1980; Murai *et al.*, 1981, 1983).

Subsequently, researchers attempted to reestablish the geology of the northern Kitakami Mountains as an accretionary complex based on the concept of plate tectonics (Minoura, 1985; Okami and Ehiro, 1988). Radiolarians obtained from mudstone and nodules therein indicated that the time of accretion was Jurassic to earliest Cretaceous (Fig. 1; Minoura and Tsushima, 1984; Matsuoka, 1987; Matsuoka and Oji, 1990; Nakae and Kamada, 2003; Suzuki and Ogane, 2004). Ehiro

[1] AIST, Geological Survey of Japan, Research Institute of Geology and Geoinformation

[2] Center for Advanced Marine Core Research, Kochi University, B200 Monobe, Nankoku, Kochi, Japan

[3] Department of Marine Resource Science, Faculty of Agriculture and Marine Science, Kochi University, B200 Monobe, Nankoku, Kochi, Japan

[*] Corresponding author: MUTO, S., Central 7, 1-1-1 Higashi, Tsukuba, Ibaraki 305-8567, Japan. Email: s-muto@aist.go.jp

et al. (2005) redefined the North Kitakami Belt as the geotectonic division for the area where the Jurassic accretionary complex is distributed in the northern Kitakami Mountains, and this definition is widely used today (Isozaki *et al.*, 2010; Kojima *et al.*, 2016; Ehiro *et al.*, 2017) (Fig. 1A).

The Jurassic accretionary complex of the North Kitakami Belt has been compared with accretionary complexes in Southwest Japan, in particular, that of the Southern Chichibu Belt (Yamakita and Otoh, 2000; Otoh and Sasaki, 2003; Ehiro *et al.*, 2008; Takahashi *et al.*, 2016). While the lithofacies and age of the Southern Chichibu Belt has been extensively studied (Matsuoka *et al.*, 1998 and references therein), the North Kitakami Belt is less well studied. This is partly due to the difficulty of obtaining radiolarians from rocks of the North Kitakami Belt, which are generally affected by Cretaceous plutons that intrude throughout the Kitakami Mountains. Although detrital zircon chronology has recently been adopted to estimate the time of accretion (e.g., Uchino, 2017, 2019; Ueda *et al.*, 2018; Fig. 1), age data remain scarce compared to the Jurassic accretionary complex in Southwest Japan.

The first author (Muto, S.) has conducted surveys to produce the 1: 50,000 geological map of the "Kado" District for the Quadrangle Series of the Geological Survey of Japan, AIST. During the investigation, we obtained new age data of radiolarians and detrital zircons. In this study, we present new information on the lithology and age of the accretionary complex distributed in the northeast part of the North Kitakami Belt in the upper reaches of the Akka River. Based on field observation and mapping, we here update the tectonostratigraphic divisions in the study area. Furthermore, we attempt regional correlations between the North Kitakami Belt and the Southern Chichibu Belt on the basis of lithology and age data.

2. Geological outline

The studied area is in the upper reaches of the Akka River in Iwaizumi Town, Iwate Prefecture, Japan. An area including part of the present study area was mapped by Sugimoto (1974) (Fig. 2). Subsequently, Takahashi *et al.* (2016) reassessed the geological division by Sugimoto (1974) based on the concept of subduction-accretion and recognized four tectonostratigraphic units bounded by thrusts. These are, in structurally descending order, the Otori Unit (coherent facies; chert and mudstone), the Seki Unit (coherent facies; chert, mudstone and sandstone), the Takayashiki Unit (mixed facies; mudstone, chert, sandstone, basalt and limestone) and the Akka Unit (coherent facies; basalt and limestone) (Fig. 2). Recently, as a result of surveys mainly in the Rikuchu-Seki District located north of our study area, Nakae *et al.* (2021) proposed that the Seki Unit should be divided into two tectonostratigraphic units; the upper Kassenba Complex (coherent facies; chert, mudstone and sandstone) and the lower Seki Complex (coherent facies; chert and mudstone)

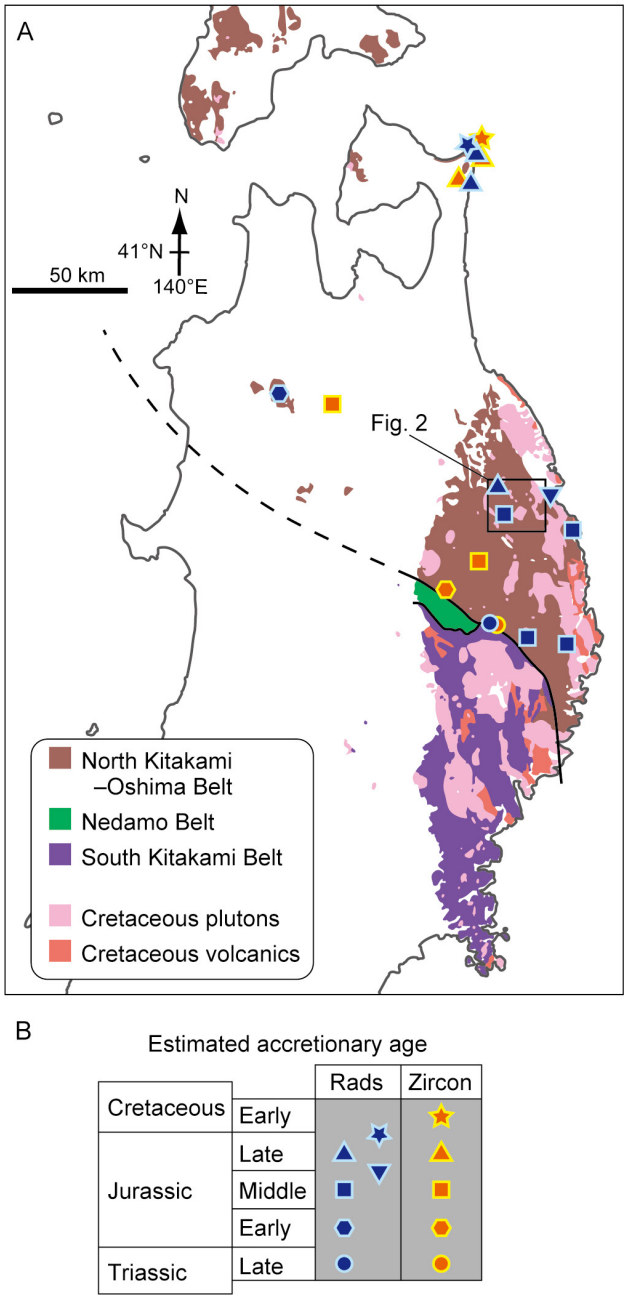

Fig.1 Geology of the basement rocks of northern Tohoku Region (modified from Geological Survey of Japan, AIST, 2020). Age data of the accretionary complex are based on the compilation by Uchino and Suzuki (2020). Rads: radiolarian fossils.

(note that "Complex" in Nakae *et al.* (2021) is equivalent to "Unit" in Takahashi *et al.* (2016)) (Fig. 2). Nakae *et al.* (2021) also combined the Takayashiki and Akka units of Takahashi *et al.* (2016) as the Takayashiki Complex and defined an additional tectonostratigraphic unit, the Kayamori Complex, structurally below the Takayashiki Complex (Fig. 2).

The present study targets the Otori Unit, the Seki

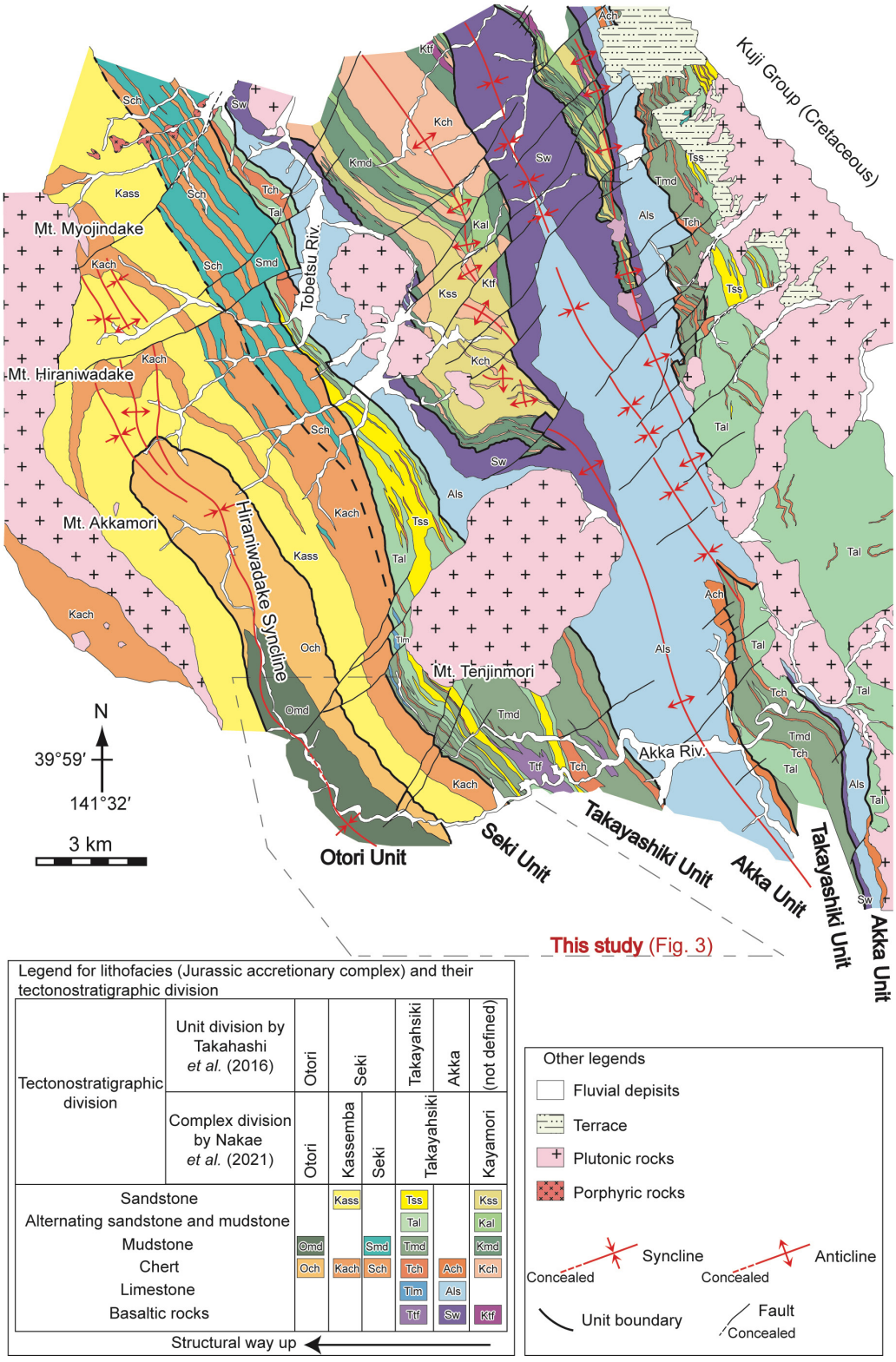

Fig.2 The geology of the North Kitakami Belt in the Akka–Kuji area (modified from Ehiro *et al.*, 2008, a simplified version of Sugimoto, 1974; partly corrected according to the original figure in Sugimoto, 1974). Unit boundaries (thrust faults) are based on the tectonostratigraphic unit division by Takahashi *et al.* (2016). The boundary between the Seki and Kassenba complexes of Nakae *et al.* (2021) (not classified as a unit boundary in Takahashi *et al.*, 2016) is shown in broken thick lines. The Seki Formation east of the Akka Unit in the northeast part (sensu Sugimoto, 1974) is ascribed to the Takayashiki Unit according to Nakae *et al.* (2021). The study area of this paper is shown in broken lines. The tectonostratigraphy and the legend and labels for lithofacies of the Jurassic accretionary complex is explained in the bottom left diagram.

Unit and the western margin of the Takayashiki Unit of Takahashi *et al.* (2016) (corresponding respectively to the Otori Complex, the Kassenba and Seki complexes and the western margin of the Takayshiki Complex of Nakae *et al.*, 2021). Below, we will conform to the nomenclature by Takahashi *et al.* (2016), since the present study area overlaps with the area studied therein.

3. Methods

3. 1 Microfossils

We investigated one mudstone sample, four siliceous mudstone samples and two manganese nodule samples for extraction of radiolarians (Table A1). Radiolarians were obtained by two different acid treatment depending on the lithology of the sample. Mudstones and siliceous mudstones were crushed into cm-size pieces and treated with 5 % hydrofluoric (HF) acid for 24 h. Manganese nodules were crushed in the same way and treated with 36 % hydrochloric (HCl) acid for 24 h. The residues were rinsed, dried and prepared into slides. Some radiolarians were picked from the residue for photography by a scanning electron microscope (SEM; JSM-6610LV, JEOL GmbH) at the Geological Survey of Japan, AIST.

We also obtained conodonts from chert by observation of cleaved rock pieces under a stereoscopic microscope (the "chip method"; Muto *et al.*, 2018). Well-preserved specimens were imaged by X-ray microtomography using an X-ray microscope (ZEISS Xradia 410 versa) equipped with a L8121-03 SEL X-ray source of Hamamatsu Photonics K.K. at the Center for Advanced Marine Core Research (Kochi Core Center), Kochi University, following the procedures in Muto *et al.* (2021).

3. 2 Detrital zircon chronology

Detrital zircons were analyzed for two sandstone samples (Table A1). Zircons were obtained from sandstone samples by Kyoto Fission-Track Co. Ltd. Zircon U–Pb dating was conducted at the Hirata-Lab. of the University of Tokyo by laser ablation inductively coupled plasma mass spectrometry (LA-ICP-MS). The LA part was CARBIDE (LIGHT CONVERSION) and the ICP-MS part was New Plasma Ⅱ (Nu instruments). Ablation pit size was 10 μm, energy density was 3.2 J/cm^2, and pulse repetition rate was 10 Hz. Laser ablation was conducted on polished sections of zircons embedded in PFA Teflon sheets. Analyses were performed after one-shot cleaning. The details of the analysis are described in Iizuka and Hirata (2004) and Hirata *et al.* (2005). Primary standard was the Plešovice zircon with a ^{238}U–^{206}Pb age of 337.13 ± 0.37 Ma (Sláma *et al.*, 2008). Secondary standard was the standard zircon 91500 with a ^{238}U–^{206}Pb age of 1062.4 ± 0.4 Ma (Wiedenbeck *et al.*, 1995) and zircon OD-3 with a ^{238}U–^{206}Pb age of 33.04 ± 0.10 Ma (Iwano *et al.*, 2013). U–Pb age data with ^{238}U–^{206}Pb age/^{235}U–^{207}Pb age ratio between 90 % and 110 % were regarded as concordant age data, following a preceding study on detrital zircons from clastic rocks within a Jurassic accretionary complex (Tokiwa *et al.*, 2019). The weighted mean age of the youngest cluster comprising two or more grains (YC1σ; Dickinson and Gehrels, 2009) and the age of the youngest single grain (YSG) were considered for estimation of accretionary age.

4. Geology of the Otori Unit

The Otori Unit (Takahashi *et al.*, 2016) was recognized between the conspicuous chert–clastic sequence of the Seki Unit in the east and the western edge of the study area (Fig. 3). The western limit of the unit cannot be defined in the present study. Based on lithological assemblages, we subdivided the Otori Unit into two subunits: the Okoshizawa and Osakamoto subunits in structurally ascending order. These two subunits mostly correspond to the Otori and Osakamoto formations of Sugimoto (1974), respectively. Both Takahashi *et al.* (2016) and Nakae *et al.* (2021) regarded that these two formations compose a single tectonostratigraphic unit composed of stacked up slices of coherent strata. However, only a minor portion of the Osakamoto Formation (*sensu* Sugimoto, 1974) was mapped by the two studies. Our investigation showed that the Osakamoto Formation is a mixed facies and is structurally different from the mostly coherent Otori Formation. Therefore, we differentiate these two as subunits.

4. 1 Okoshizawa Subunit

Definition—The Okoshizawa Subunit (named after "Okoshizawa", Japanese for Okoshi Stream) is the dominantly coherent facies of mainly chert and siliceous mudstone that occupies the structurally lower part of the Otori Unit (Figs. 3–5). The structural base of the subunit is defined at the base of mudstone dominant lithofacies which lies structurally above the top of the bedded sandstone of the Seki Unit. The structural top of the subunit is defined at the top of the chert–siliceous mudstone sequence that can be traced laterally for over 10 km from Okoshi Stream to the Orikabe River. The mudstone-dominant lithofacies with a narrow distribution at the structural base of the Otori Unit and the mixed to broken facies of mudstone and sandstone in the north to southeast of Otori is included in this subunit. The Okoshizawa Subunit mostly corresponds to the Otori Formation of Sugimoto (1974).

Type locality—The upper reaches of Okoshi Stream (Fig. 4).

Lithofacies—This subunit is composed largely of structurally repeating chert and siliceous mudstone. Mixed to broken facies of mudstone and sandstone is present in the southeast part of the subunit. In addition, chert breccia, although limited in distribution, occurs characteristically around Okoshi Stream in the structurally lower part. Below, the lithology of the Okoshizawa Subunit is explained generally in the order of abundance.

Chert is bedded and is mainly grey (Fig. 6A). It is

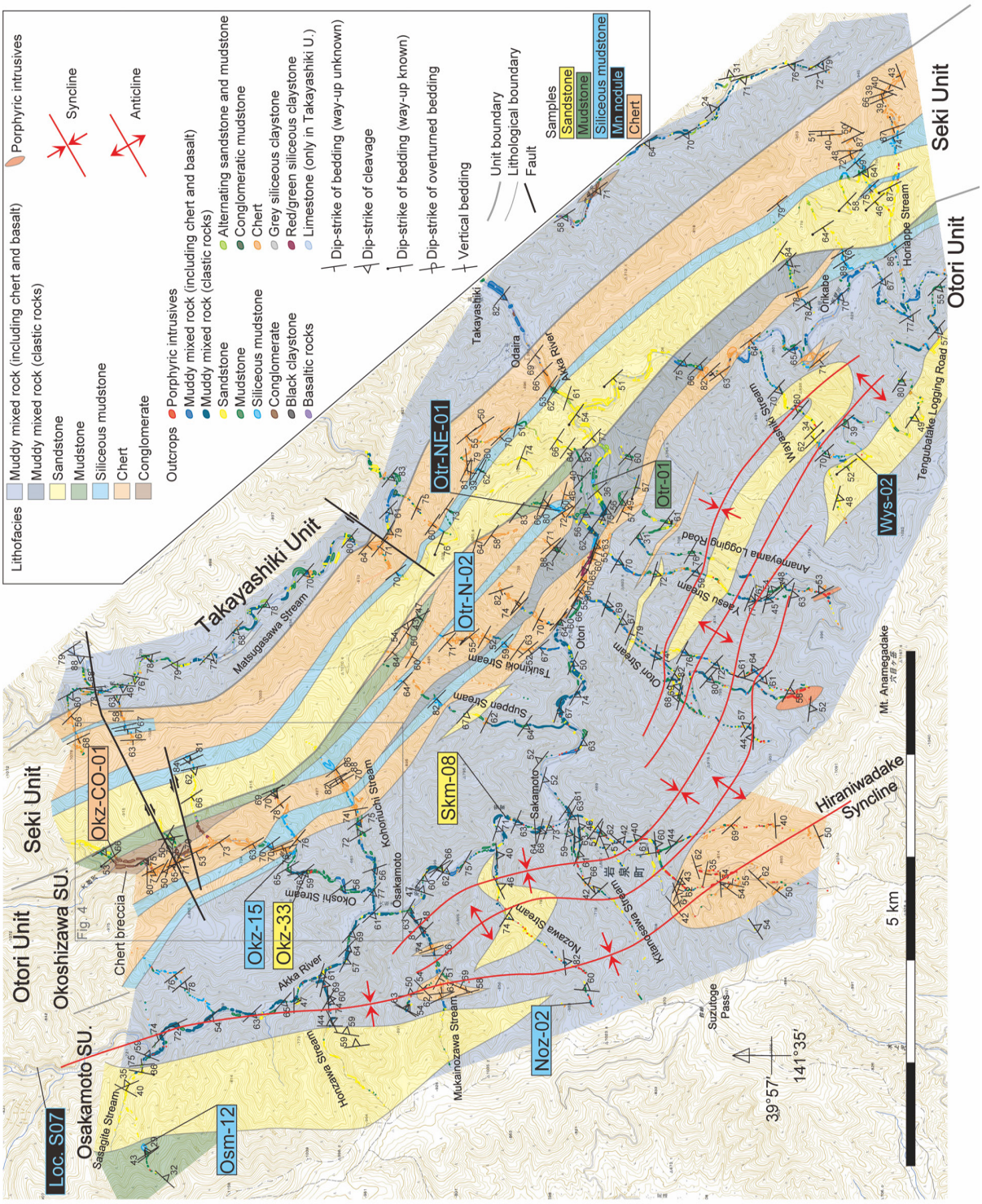

Fig. 3 Geological map of the studied area. Base map from 1: 25,000 topographic map "Akkamori", "Rikuchu-Itsukaichi", "Hashigami" and "Akka" by the Geospatial Authority of Japan. SU.: Subunit.

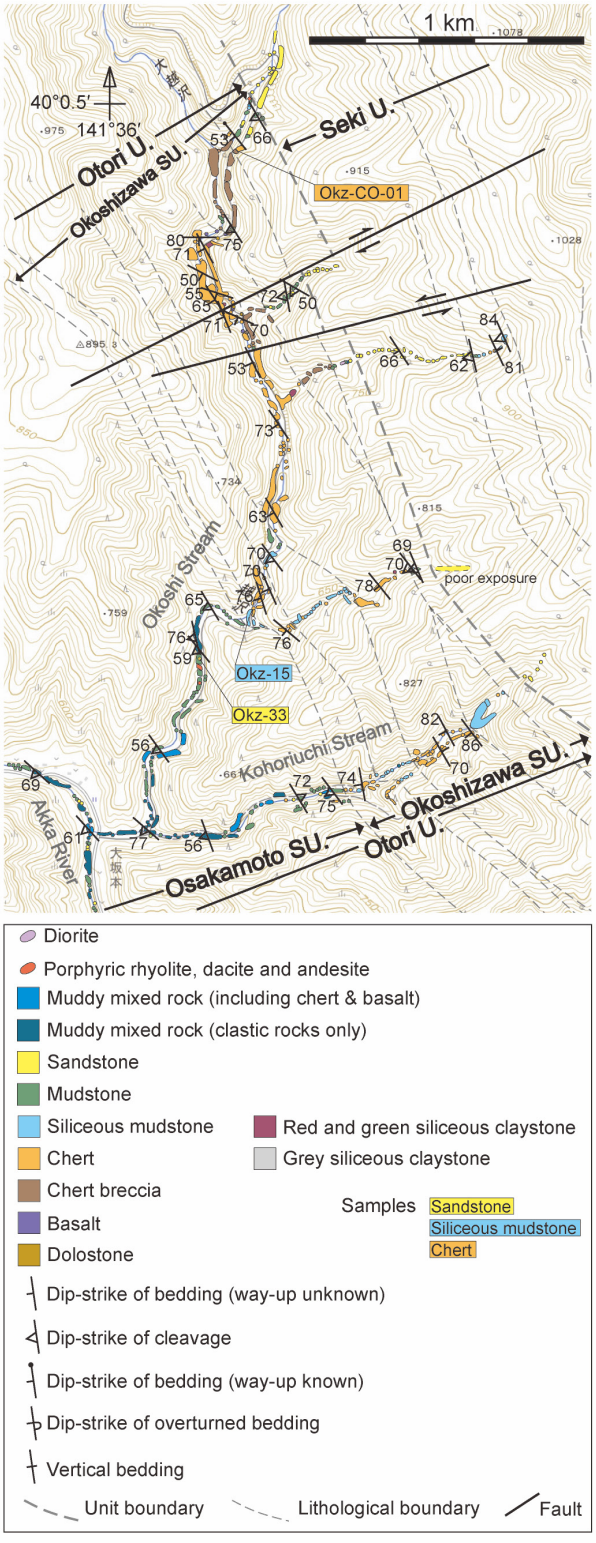

Fig. 4 Geological traverse map around Okoshi Stream. Base map from 1: 25,000 topographic map "Akkamori" and "Rikuchu-Itsukaichi" by the Geospatial Authority of Japan. U.: Unit; SU.: Subunit. Str.: Stream; Riv.: River.

accompanied at the basal part by basaltic volcaniclastics, dolostone partly interbedded with greenish grey chert (Fig. 6D), green siliceous claystone (Fig. 6E) and red siliceous claystone (Fig. 6F). Within the chert sequence, a characteristic horizon of black carbonaceous claystone is present (Fig. 6G), which is known to be the Permian–Triassic boundary (Ehiro *et al.*, 2008; Takahashi *et al.*, 2009). In some places, the black claystone is overlain by grey siliceous claystone. In thin section, chert is mostly made up of microcrystalline quartz matrix and radiolarian tests that are recrystallized to various degrees (Fig. 7A). Dolostone is composed of euhedral dolomite with minor microcrystalline quartz matrix (Fig. 7C, D). Dolostone also contains irregular-shaped basaltic rock fragments (Fig. 7D). Basaltic volcaniclastics are composed of basaltic rock fragments and tuff (Fig. 7E). The former partly shows chilled-margins and vesicular texture implying fragmented lava.

Siliceous mudstone is light grey and weakly to strongly bedded (Fig. 6B). It commonly forms steep and jagged cliffs like chert, but can be distinguished from the latter by the tendency to split parallel to or at a low angle to the bedding plane when struck with a hammer. In thin section, it is composed of clay minerals, microcrystalline quartz and abundant radiolarian tests (Fig. 7B). Silty laminae of quartz and micaceous minerals may occur.

Chert breccia is grey, completely consolidated and its jagged outcrop surface looks like that of chert. On fresh surfaces, angular and poorly sorted chert pebbles are evident. In some outcrops, chert breccia was found in contact with mudstone and conglomeratic mudstone without a slip plane or any apparent parting separating them (Fig. 6I). In thin section, chert breccia is composed almost entirely of poorly sorted angular chert pebbles and granules that are recrystallized to various degrees (Fig. 7F). The chert pebbles and granules are interlocked and no matrix is observed. Rare mudstone clasts may be present.

Ehiro *et al.* (2008) ascribed this chert breccia to the Kassenba Formation (Sugimoto, 1974), which corresponds to the upper part of the Seki Unit. However, it is included in the Otori Unit based on the following observations. First, the chert breccia is structurally underlain by mudstone in Okoshi Stream, which in turn is underlain by bedded sandstone of the Seki Unit (Figs. 3, 4, 5). Second, the chert breccia is associated with conglomeratic mudstone, which is separated from bedded sandstone of the Seki Unit by chert in the area north of Otori (Figs. 3, 5). In both cases, the Otori–Seki unit boundary should be placed at the top of the bedded sandstone, because the upper part of the Seki Unit is composed almost exclusively of bedded sandstone. Thus, the boundary is below the chert breccia.

Sandstone occurs in the southeast part of the subunit, and is either massive or bedded. It ranges from bodies that are 100 m thick to mm-size fragments in mudstone matrix.

Mudstone is black or dark grey and generally shows weak cleavage. It occurs mainly in two distributions: in the northern part of the subunit at its structural base

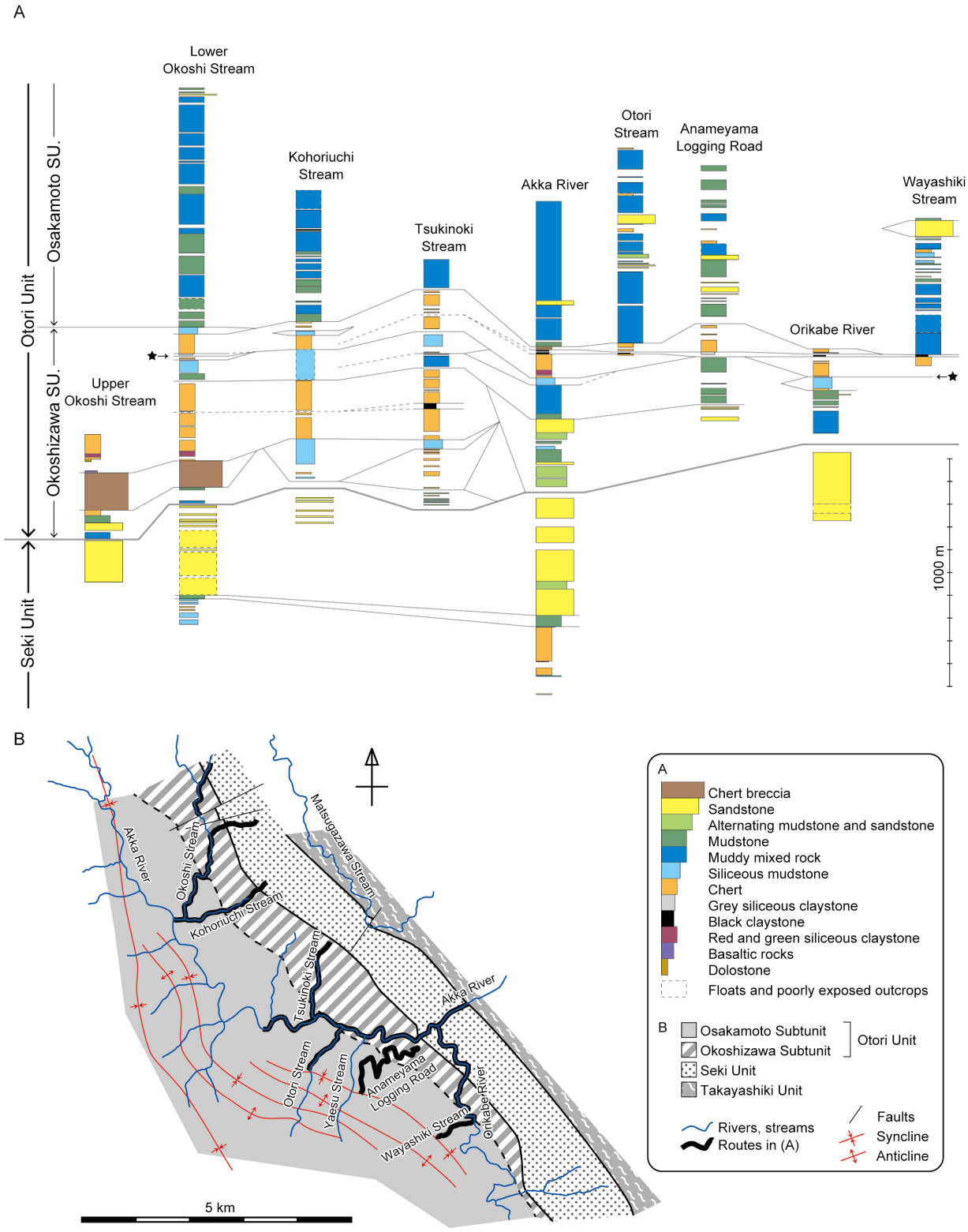

Fig. 5 (A) Tectonostratigraphic logs of the studied area and (B) index map (simplified version of Fig. 3). SU.: Subunit. The black star in A indicates the thrust referred to in p.10.

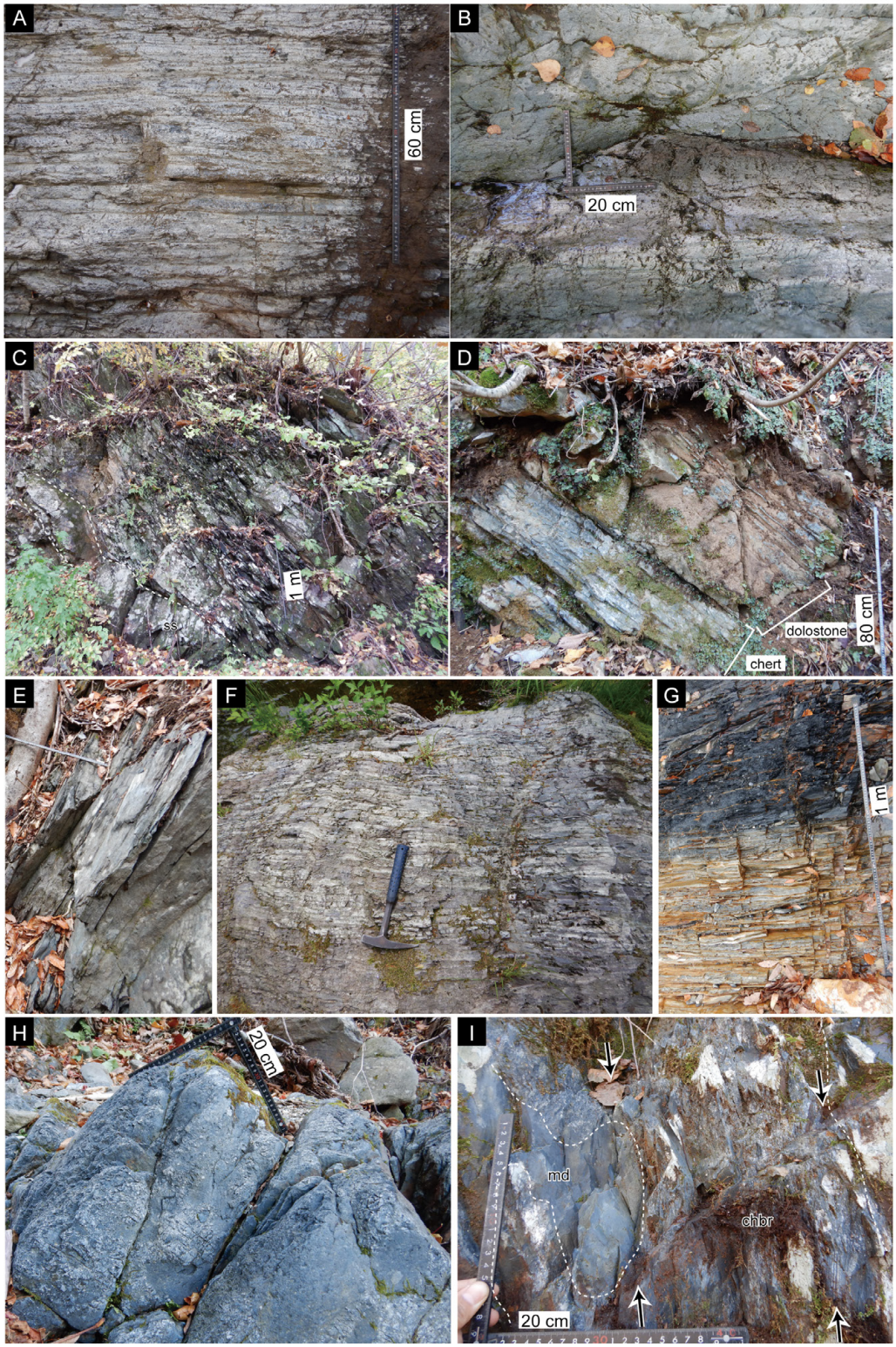

Fig. 6 Outcrop photographs of the main lithologies of the Okoshizawa Subunit. (A) Bedded chert. (B) Siliceous mudstone. (C) Mudstone with broken sandstone bed (ss). (D) Alternating chert and dolostone. (E) Green siliceous claystone. (F) Red to brownish red siliceous claystone. The hammer is 33 cm long. (G) Sequence of grey bedded chert, grey siliceous claystone and black carbonaceous claystone at the Permian–Triassic boundary. (H) Chert breccia. (I) Boundary between chert breccia (chbr) and mudstone (md) (thin broken line). Cleavage planes (partly parallel to lamination in the bottom right) are indicated by arrows. See Table A2 for location.

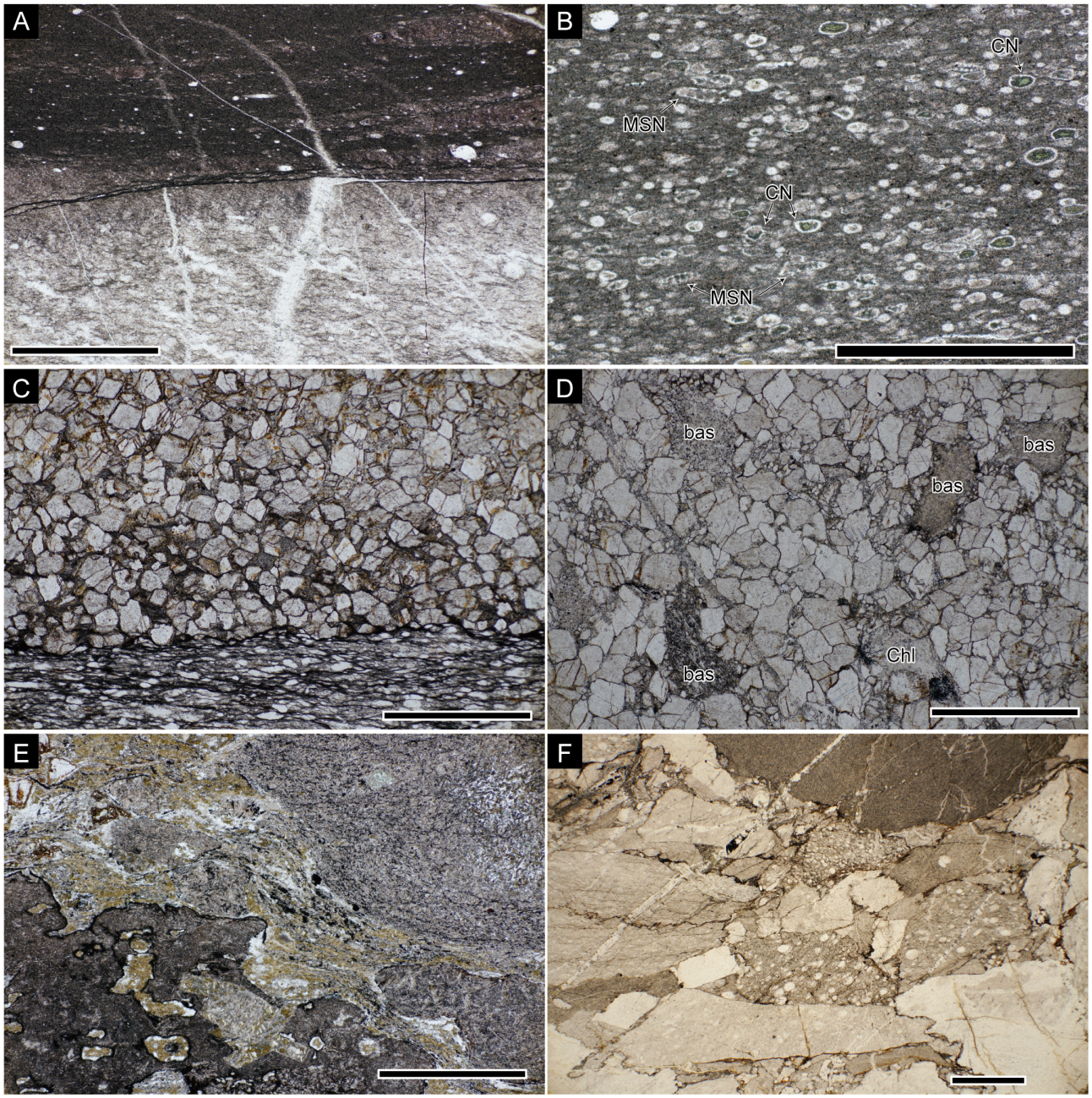

Fig. 7 Thin section micrographs of the main lithologies of the Okoshizawa Subunit. All pictures were taken with transmitted plane-polarized light. (A) Chert (bottom) and siliceous claystone (top) of bedded chert. (B) Siliceous mudstone including radiolarian fossils. CN: closed Nasselaria; MSN: multi-segmented Nasselaria. (C) Dolostone layer (top) with chert layer. (D) Dolostone with basaltic rock fragments (bas) and chlorite aggregates (Chl). (E) Basaltic volcaniclastic rock. (F) Chert breccia. Scale bars are 1 mm.

and in the southeast part of the subunit (Fig. 3). In the former, it is accompanied by fine sandstone and is partly conglomeratic. In the latter, it occurs as massive bodies, matrix including sandstone and beds alternating with sandstone.

Distribution—The Okoshizawa Subunit is distributed in a NW–SE trending area from Okoshi Stream to Orikabe settlement. It is thicker in the northwestern to central part (800–950 m) compared to the southwestern part (400 m) (Fig. 5). According to Sugimoto (1974) and Nakae *et al.* (2021), this subunit extends further north for about 6 km, where it forms a syncline along with the Osakamoto Subunit (the Hiraniwadake Syncline).

Structure—Overall, the structure of the Okoshizawa Subunit deduced from orientation of bedding planes and cleavage planes is homoclinal with a NW–SE strike and

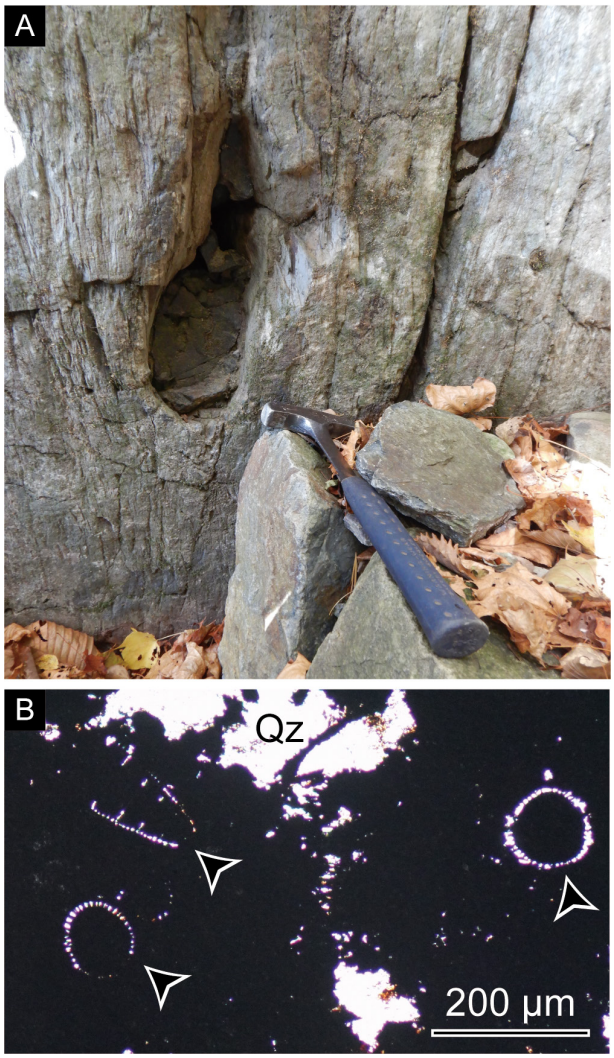

Fig. 8 Outcrop photograph (A) and thin section micrograph (B) of the nodule sample (Otr-NE-01) that yielded radiolarians. The hammer in the bottom right of (A) is 33 cm long. Arrows in (B) indicate well-preserved radiolarians. Scale bar in (B) is 200 μm. Qz: quartz cement.

50–70° dip to the SW. Chert and siliceous mudstone form a coherent sequence and is repeated by thrusts in the northern to central part of the subunit. The thrusts and related faults cut the bedding of the chert–siliceous mudstone sequence at low angles. For example, the thrust at the base of the structurally highest chert (denoted by the black star in Fig. 5) runs above the Permian–Triassic black claystone horizon in Okoshi Stream, is well below the black claystone horizon in Otori (Akka River in Fig. 5A), moves up above the black claystone horizon in the Aname-yama Logging Road and moves back below the black claystone in Orikabe River (Fig. 5A). Due to the nature of these faults, the apparent thickness of chert and siliceous claystone in the Okoshizawa Subunit is laterally variable (Fig. 3).

Age—Carboniferous to Triassic conodonts have been reported from chert (Toyohara *et al.*, 1980; Ehiro *et al.*, 2008; Takahashi *et al.*, 2016; Muto *et al.*, 2021), although not many specimens have been illustrated. Suzuki *et al.* (2007) reported radiolarians of the *Striatojaponocapsa plicarium* Zone (JR4 of Matsuoka and Ito, 2019; Bajocian to early Bathonian, Middle Jurassic) from manganese nodules within siliceous mudstone.

We obtained conodont fossils from chert (Okz-CO-01) in the lowermost part of the Okoshizawa Subunit. This chert is directly in contact with chert breccia, but their relationship was not clear due to poor outcrop condition. They are structurally below a chert-dominant sequence of Paleozoic age (Ehiro *et al.*, 2008; Muto *et al.*, 2021). The conodonts obtained in this study are *Misikella longidentata*, *Paragondolella* cf. *inclinata*, *Paragondolella polygnathiformis* and *Sephardiella mungoensis* (Fig. 11). The cooccurrence of these conodonts indicates that the chert is earliest Carnian in age (Chen *et al.*, 2016). Therefore, this chert and accompanying chert breccia form a thrust sheet structurally underlying Paleozoic chert exposed around Okoshi Stream. It is inferred that the chert breccia originated from the collapse of Triassic chert, possibly on the trench-slope.

We obtained well-preserved radiolarians from a black manganese nodule (sample Otr-NE-01) within grey siliceous mudstone (Fig. 8A). In thin section, the manganese nodule contains radiolarians that retain microscopic ornamentations (Fig. 8B). The radiolarians include *Diacanthocapsa*? *operculi*, *Eucyrtidiellum unumaense*, *Gongylothorax siphonofer*, *Japonocapsa fusiformis*, *Protunuma fusiformis* and *Striatojaponocapsa synconexa* (Plate 1). According to the detailed stratigraphic work by Hatakeda *et al.* (2007), *S. synconexa* occurs in the upper part of the *Striatojaponocapsa plicarum* Zone (JR4: Bajocian to lower Bathonian) to the lower part of the *Striatojaponocapsa conexa* Zone (JR5: upper Bathonian to Callovian) of Matsuoka and Ito (2019). Other species, such as *J. fusiformis* and *E. unumaense* occur in biozones JR4 and JR5 (Matsuoka, 1995; Matsuoka and Ito, 2019). Consequently, the radiolarian assemblage indicates the upper JR4 to lower JR5 (the Bathonian). Occurrences of *Diacanthocapsa*? *operculi*, *Gongylothorax siphonofer* and *Protunuma fusiformis* are consistent with the age assignment.

Two siliceous mudstone samples (Otr-N-02 and Okz-15) also yielded radiolarians, although preservation was rather poor (Plates 2, 3). Both samples yielded specimens that are possibly a species of Williriedellidae. According to O'Dogherty *et al.* (2017), the occurrence range of the family Williriedellidae is early Pliensbachian–Maastrichtian. Although the age of the siliceous mudstone samples cannot be determined in detail, it does not contradict with the age of the manganese nodule sample.

4. 2 Osakamoto Subunit

Definition—The Osakamoto Subunit is the mixed

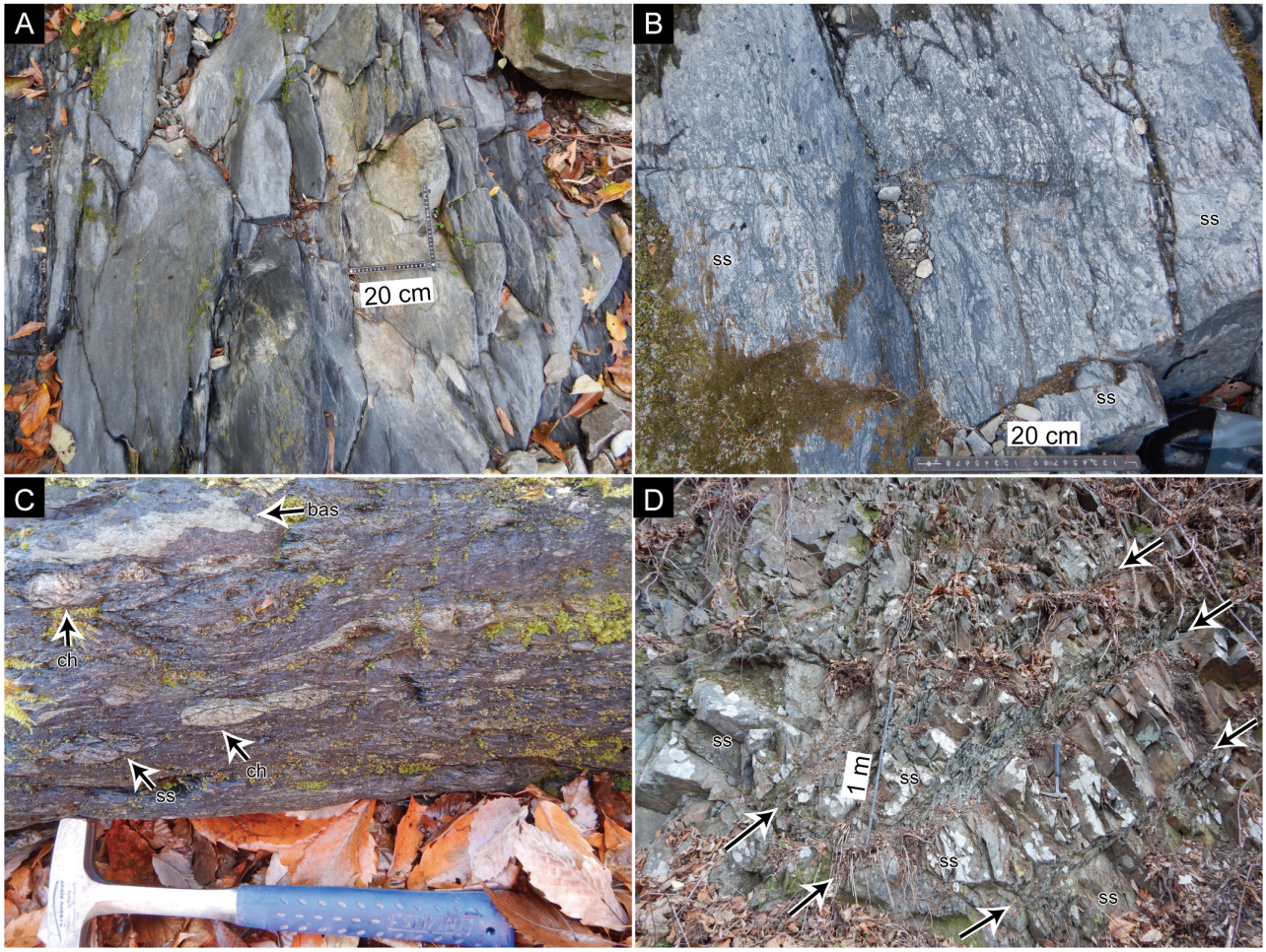

Fig. 9 Outcrop photographs of the main lithologies of the Osakamoto Subunit. (A) Mudstone with no visible rock fragments. (B) Mudstone with abundant sandstone fragments. (C) Muddy mixed rock including basaltic rocks (bas), chert (ch) and sandstone (ss) fragments. The hammer is 33 cm long. (D) Coherent sandstone (ss) with mudstone interbeds. Bedding planes are indicated by arrows. See Table A2 for location.

facies of mudstone, sandstone, siliceous mudstone, chert and rare basaltic rocks that occupies the structurally upper part of the Otori Unit. The structural base of the subunit is the same as the structural top of the Okoshizawa Subunit. The structural top of the subunit is not defined. This subunit includes the Osakamoto Formation of Sugimoto (1974). Sugimoto (1974) assigned the sandstone dominant lithofacies northwest of Osakamoto in the northwestern edge of the study area to the Kassenba Formation (i.e., the upper part of the Seki Unit in Takahashi *et al.*, 2016). However, the sandstone northwest of Osakamoto is mostly massive, while that of the Seki Unit is characterized by prominent bedding. In addition, we obtained radiolarians indicating the Bathonian (as detailed in the Age section) from siliceous mudstone in the northwest edge of the study area, structurally below the massive sandstone. Since the mudstone of the Seki Unit is likely to be the Kimmeridgian (middle Upper Jurassic) (Nakae and Kamada, 2003), it is more reasonable to include the massive sandstone and muddy rocks in the northwestern edge of the study area in the Otori Unit.

Type locality—Along the Akka River near Osakamoto settlement and the lower reaches of Okoshi Stream (Fig. 4).

Lithofacies—The Osakamoto Subunit is a mixed facies dominantly composed of mudstone and muddy mixed rocks. Mappable bodies of sandstone and chert are present within this subunit. Below, the lithology of the Osakamoto Subunit is explained generally in the order of abundance.

Mudstone is black to dark grey and generally has weak scaly cleavage (Fig. 9A). Bedding planes and other sedimentary structures are usually not observed. In thin section, it is composed of clay minerals, quartz and feldspar grains and opaque matter (Fig. 10A). Sandstone fragments are present even in mudstone with no visible rock fragments at the outcrop. Opaque seams are developed within mudstone.

Two types of muddy mixed rocks are present within the Osakamoto Subunit. The first is composed of sandstone within mudstone matrix (Fig. 9B). The majority of the muddy mixed rock in the subunit is of this type. Sandstone

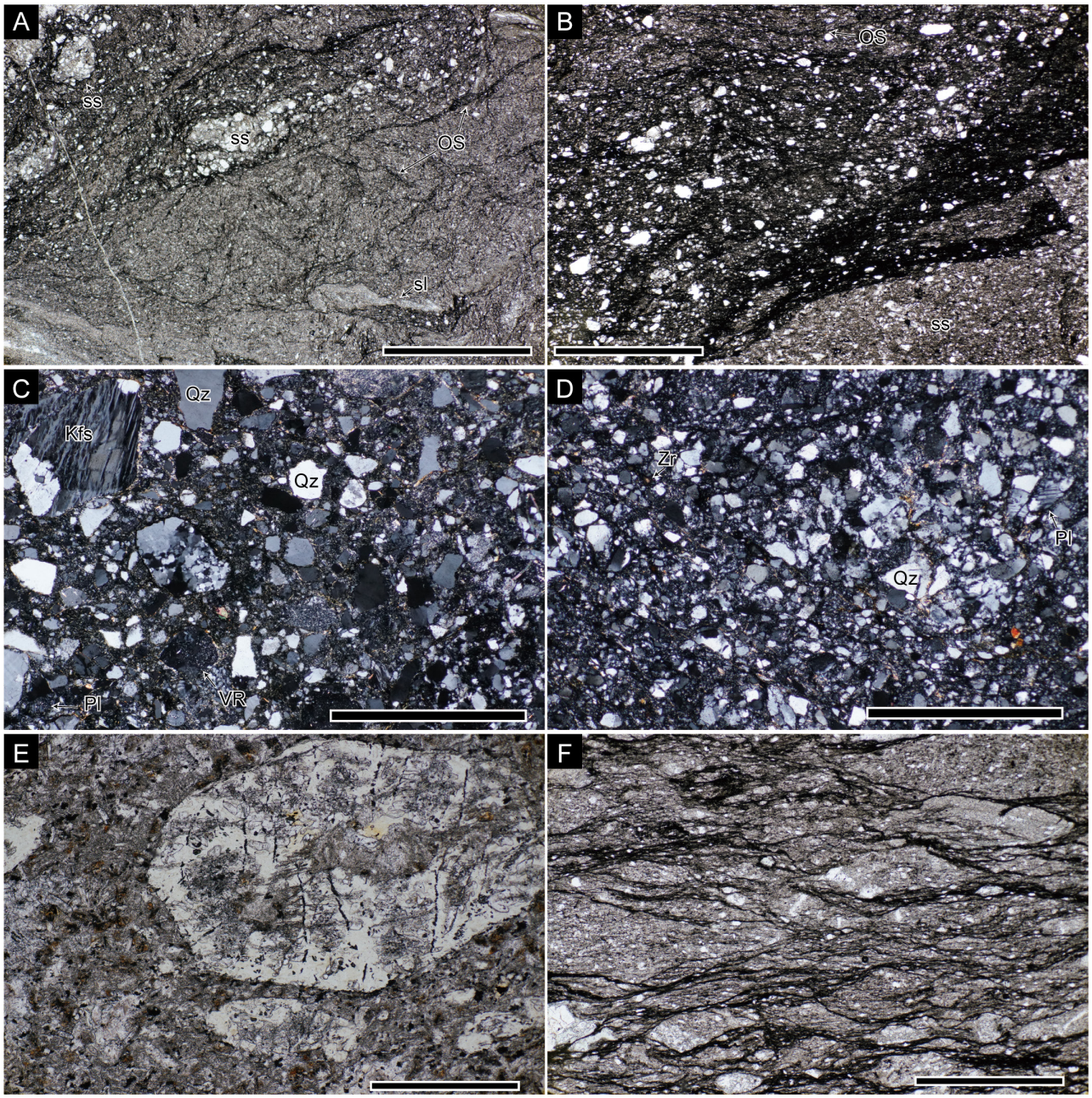

Fig. 10 Thin section micrographs of the main lithologies of the Osakamoto Subunit. (A) Mudstone with no observable rock fragments at the outcrop (same as Fig. 9A). OS: opaque seams; ss: sandstone; sl: fragmented sandstone laminae. (B) Mudstone with abundant sandstone fragments. (See above for abbreviations.) (C, D) Sandstone within muddy mixed rock. Kfs: K-feldspar in rock fragment; Qz: quartz; Pl: plagioclase; Zr: zircon; VC: volcanic rock fragment. (E) Altered basalt. A large octagonal section of a phenocryst (now replaced by chlorite and carbonate) occupies the top right of the picture. (F) Muddy mixed rock with sheared microstructures. (A), (B), (E) and (F) were taken with transmitted plane-polarized light. (C) and (D) were taken with cross-polarized light. Scale bars are 1 mm.

ranges from mm-size fragments to m-size blocks. The boundary between sandstone and mudstone matrix is either irregular or sharp and mixing may have occurred both before and after consolidation. In thin section, the components of this type of muddy mixed rock are the same as that of mudstone, except that the proportion of sandstone is much greater (Fig. 10B). The other type of muddy mixed rock contains chert and minor basaltic rocks in addition to sandstone (Fig. 9C). However, chert and basaltic rocks are minor compared to sandstone. Asymmetric shear fabric was observed in thin section of a mixed muddy rock sample adjacent to a block of basaltic rock (Fig. 10F).

Sandstone is grey and occurs as mm-size fragments to

>200 m-thick bodies. It is generally massive with mud seams, but bedded varieties are present in the southeast part of the study area (Fig. 9D). In thin section, sandstone is composed of grains of quartz, plagioclase, K-feldspar, lithic fragments and other minor minerals such as zircons (Fig. 10C, D).

Chert is grey, white or black and occurs as mm-size fragments to m-size blocks or as m-thick to laterally traceable bodies that are mostly 10–50 m thick. In the southwest part of the study area, a mappable body of chert attains >400 m in apparent thickness around the Hiraniwadake Syncline axis (Fig. 3). Chert is generally bedded and sometimes recrystallized and massive. In thin section, it is composed of recrystallized radiolarian tests, microcrystalline quartz matrix and minor clay minerals.

Basaltic rocks are rare and were only found as <50 cm-thick blocks in a few localities. They are light green in colour and are composed of secondary minerals such as chlorite, other phyllosilicates such as talc and carbonate (Fig. 10E).

Siliceous mudstone is also present in the Osakamoto Subunit. It is black or grey and is either massive or bedded. The black massive varieties are very similar to mudstone and the two can be indistinguishable without observation of thin sections. Siliceous mudstone occurs as blocks within a muddy matrix, but it also appears to constitute a part of the matrix of the mixed facies.

Distribution—The confirmed distribution of this subunit is a triangular area between Osakamoto, Suzutoge Pass and Orikabe (Fig. 3). The area to the south and west has not been mapped in detail and further studies are required to determine the southwest boundary of this subunit. The distribution of this subunit closes around the Hiraniwadake Syncline axis ~500 m north of the northern edge of our study area (Sugimoto, 1974). The apparent thickness of the Osakamoto Subunit is around 1,200 m in the east wing of the Hiraniwadake Syncline near Osakamoto. It is somewhat difficult to evaluate the thickness in the central to southeastern part of the distribution due to multiple folds (see below), but the apparent thickness is at least 850 m in Otori Stream and 600 m in Wayashiki Stream, respectively (Fig. 4).

Structure—The structure of this subunit is homoclinal in the northeastern part and folded in the southwestern part (Fig. 3). The homoclinal part has cleavage planes and bedding planes with NW–SE strikes and dips of 50–80° to the southwest (Fig. 3). Sugimoto (1974) recognized a syncline in the Osakamoto Subunit along the Akka River, which is the southern part of a major NNW–SSE-trending syncline named the Hiraniwadake Syncline that extends more than 14 km from Mt. Myojindake (Fig. 2). This syncline extends throughout the newly mapped distribution of the Osakamoto Subunit (Fig. 3). In addition, two sets of second-order syncline and anticline occur in the southwest part of the Osakamoto Subunit (Fig. 3). The axes of these folds are parallel and trend NNW–SSE to NW–SE.

Age—Previously, no age constraints had been obtained from rocks of the Osakamoto Subunit. We obtained radiolarians from two black siliceous mudstone samples (Osm-12 and Noz-02) and analyzed detrital zircon U–Pb ages for two sandstone samples (Okz-33 and Skm-08).

Sample Osm-12 yielded *J.* cf. *fusiformis* and *S. synconexa* (Plate 4). As mentioned in the age section for the Otori Subunit, *S. synconexa* indicates the upper JR4 to lower JR5 (Bathonian). *Japonocapsa fusiformis* is known to co-occur with *S. synconexa* (e.g., O'Dogherty *et al.*, 2006). Hence, the sample most likely indicates the upper JR4 to lower JR5 (Bathonian). Sample Noz-02 yielded *Praezhamoidellum*? cf. *japonicum* and *J.* cf. *fusiformis* (Plate 5). According to Matsuoka and Ito (2019), *J. fusiformis* indicates the upper JR3 to lowermost JR6 (upper Aalenian–Callovian).

Detrital zircon U–Pb age was analyzed for one sandstone sample from Okoshi Stream (Okz-33) and another from Akka River near Sakamoto (Skm-08). The number of grains with concordant U–Pb ages was 61 out of 62 for Okz-33 (Table 1) and 60 out of 60 for Skm-08 (Table 2). Okz-33 included a large number of Jurassic zircons, while Skm-08 contained no Jurassic zircons (Fig. 12). Abundant Permian and Triassic zircons and minor Precambrian zircons were obtained from both samples (Fig. 12). Sample Okz-33 had a YC1σ of 171.8 ± 2.4 Ma and a YSG of 170.9 ± 3.8 Ma, while Skm-08 had a YC1σ of 223.6 ± 4.2 Ma and a YSG of 221.4 ± 5.7 Ma.

As described above, the Otori Unit has a two-story-structure with the coherent Okoshizawa Subunit occupying the structurally lower part and the mixed Osakamoto Subunit occupying the structurally upper part. While the structure and proportion of rock components of the two subunits are different, the variety of the components are almost the same; the main components in both subunits are sandstone, mudstone, siliceous mudstone, chert and rare basaltic rocks and limestone is absent in both subunits. Hence, the two subunits may have formed by different grades of mixing from the same set of lithology on an oceanic plate. Minor differences between the two subunits are the apparent absence of the stratigraphically lower part of the pelagic chert sequence (black carbonaceous claystone, red and green claystone and dolostone) and the occurrence of black siliceous mudstone in the Osakamoto Subunit.

The boundary between the two subunits is represented by the lithological boundary between chert (Okoshizawa Subunit) and muddy mixed rocks (Osakamoto Subunit) or siliceous mudstone (Okoshizawa Subunit) and muddy mixed rocks (Osakamoto Subunit) (Figs. 3, 5). In the former case, the boundary is definitely a fault, but in the latter case, the lithological boundary may be partly conformable. For example, in the lower part of Okoshi Stream, siliceous mudstone of the Otori Subunit is structurally overlain by mudstone of the Osakamoto Subunit that includes broken tuffaceous beds and no other visible blocks.

Table 1 Zircon U–Pb isotopic data for Sample Okz-33 obtained by quadrupole inductively coupled plasma mass spectrometry.

No.	Th/U	Isotopic ratios						U–Pb age (Ma)			
		$^{207}Pb/^{206}Pb$	Error 2σ	$^{207}Pb/^{235}U$	Error 2σ	$^{206}Pb/^{238}U$	Error 2σ	$^{206}Pb/^{238}U$	Error 2σ	$^{207}Pb/^{235}U$	Error 2σ
1	0.44	0.0513	0.0012	0.2934	0.0092	0.0415	0.0008	261.9	± 5.4	261.3	± 9.3
2	0.72	0.0497	0.0013	0.1896	0.0063	0.0276	0.0006	175.7	± 3.6	176.3	± 6.4
3	0.19	0.1137	0.0015	5.2859	0.1337	0.3370	0.0064	1872.5	± 41.2	1866.6	± 127.4
4	0.38	0.0492	0.0013	0.1870	0.0063	0.0275	0.0006	175.2	± 3.6	174.1	± 6.4
5	0.48	0.0497	0.0012	0.2089	0.0066	0.0305	0.0006	193.4	± 3.9	192.7	± 6.7
6	0.38	0.1118	0.0015	5.1829	0.1332	0.3358	0.0065	1866.7	± 42.0	1849.8	± 126.9
7	0.31	0.0512	0.0012	0.2836	0.0089	0.0401	0.0008	253.6	± 5.2	253.5	± 9.0
8	0.51	0.0553	0.0018	0.2714	0.0107	0.0356	0.0009	225.4	± 5.5	243.8	± 10.8
9	0.73	0.0517	0.0015	0.2961	0.0109	0.0415	0.0010	262.2	± 6.2	263.4	± 11.0
10	0.74	0.0514	0.0019	0.2164	0.0091	0.0305	0.0007	193.8	± 4.8	198.9	± 9.2
11	0.32	0.0509	0.0010	0.2860	0.0081	0.0407	0.0008	257.3	± 4.9	255.4	± 8.2
12	0.44	0.0495	0.0016	0.1961	0.0076	0.0287	0.0007	182.4	± 4.2	181.8	± 7.7
13	0.49	0.0490	0.0017	0.2066	0.0084	0.0306	0.0007	194.2	± 4.7	190.7	± 8.5
14	0.53	0.0522	0.0017	0.2889	0.0116	0.0401	0.0010	253.4	± 6.4	257.7	± 11.7
15	0.54	0.0488	0.0012	0.1995	0.0064	0.0296	0.0006	188.1	± 3.8	184.7	± 6.5
16	0.54	0.0524	0.0014	0.2584	0.0089	0.0357	0.0008	226.3	± 4.9	233.4	± 9.0
17	0.29	0.0537	0.0014	0.3228	0.0109	0.0436	0.0009	274.9	± 6.1	284.0	± 11.0
18	0.62	0.0516	0.0013	0.2832	0.0093	0.0398	0.0008	251.6	± 5.3	253.2	± 9.4
19	0.46	0.0494	0.0017	0.2023	0.0082	0.0297	0.0007	188.5	± 4.5	187.0	± 8.3
20	0.70	0.0486	0.0013	0.2074	0.0071	0.0309	0.0006	196.2	± 4.1	191.4	± 7.2
21	0.71	0.0490	0.0016	0.2025	0.0063	0.0299	0.0007	190.1	± 4.8	187.2	± 6.4
22	0.16	0.1136	0.0018	5.2279	0.0671	0.3337	0.0074	1856.2	± 47.3	1857.2	± 65.9
23	0.47	0.1140	0.0018	5.3233	0.0824	0.3384	0.0080	1878.8	± 51.1	1872.6	± 80.4
24	0.44	0.1137	0.0019	5.2465	0.1010	0.3344	0.0086	1859.5	± 55.5	1860.2	± 97.7
25	0.35	0.0500	0.0014	0.1998	0.0052	0.0290	0.0007	184.1	± 4.4	185.0	± 5.3
26	0.51	0.0520	0.0014	0.2951	0.0073	0.0411	0.0010	259.9	± 6.3	262.6	± 7.4
27	0.73	0.0493	0.0014	0.2055	0.0056	0.0302	0.0007	191.9	± 4.6	189.7	± 5.7
28	0.56	0.0503	0.0015	0.2136	0.0059	0.0308	0.0007	195.5	± 4.8	196.6	± 6.0
29	0.57	0.0505	0.0015	0.2157	0.0062	0.0310	0.0008	196.7	± 4.9	198.4	± 6.3
30	0.60	0.0517	0.0014	0.2157	0.0054	0.0302	0.0007	192.1	± 4.6	198.3	± 5.5
31	0.73	0.0519	0.0016	0.2896	0.0083	0.0405	0.0010	255.7	± 6.5	258.3	± 8.4
32	0.54	0.0501	0.0012	0.1858	0.0040	0.0269	0.0006	170.9	± 3.8	173.0	± 4.0
33	0.42	0.0520	0.0016	0.2956	0.0085	0.0412	0.0010	260.1	± 6.7	262.9	± 8.6
34	0.59	0.0502	0.0020	0.2244	0.0088	0.0324	0.0009	205.4	± 5.9	205.6	± 8.9
35	0.15	0.0536	0.0011	0.3879	0.0071	0.0524	0.0012	329.4	± 7.5	332.8	± 7.2
36	0.26	0.1133	0.0017	5.3471	0.0657	0.3419	0.0074	1895.9	± 47.8	1876.4	± 64.6

Continued.

Table 1 Continued.

No.	Th/U	Isotopic ratios						U–Pb age (Ma)			
		$^{207}Pb/^{206}Pb$	Error 2σ	$^{207}Pb/^{235}U$	Error 2σ	$^{206}Pb/^{238}U$	Error 2σ	$^{206}Pb/^{238}U$	Error 2σ	$^{207}Pb/^{235}U$	Error 2σ
37	0.61	0.0569	0.0013	0.5727	0.0118	0.0729	0.0017	453.9	± 11.0	459.8	± 11.9
38	0.57	0.0501	0.0011	0.1921	0.0034	0.0278	0.0006	176.7	± 3.8	178.4	± 3.4
39	0.27	0.0503	0.0014	0.2175	0.0056	0.0313	0.0007	198.8	± 4.8	199.8	± 5.7
40	0.36	0.0505	0.0009	0.2234	0.0031	0.0321	0.0007	203.5	± 4.3	204.7	± 3.2
41	0.62	0.0511	0.0018	0.2963	0.0107	0.0420	0.0012	265.5	± 7.5	263.5	± 10.8
42	0.56	0.0546	0.0016	0.4382	0.0139	0.0582	0.0016	364.6	± 10.2	369.0	± 14.0
43	0.28	0.1139	0.0014	5.2008	0.0799	0.3311	0.0074	1843.6	± 47.8	1852.7	± 78.1
44	0.15	0.1162	0.0014	5.5129	0.0859	0.3438	0.0078	1905.0	± 49.9	1902.6	± 83.7
45	0.60	0.0502	0.0024	0.1884	0.0092	0.0272	0.0009	173.1	± 5.5	175.3	± 9.3
46	0.63	0.0503	0.0010	0.1876	0.0037	0.0270	0.0006	172.0	± 3.8	174.6	± 3.8
47	0.44	0.0513	0.0022	0.2622	0.0119	0.0371	0.0012	234.7	± 7.5	236.5	± 12.0
48	0.33	0.0493	0.0009	0.1903	0.0034	0.0280	0.0006	177.7	± 3.8	176.9	± 3.5
49	0.61	0.0507	0.0023	0.2877	0.0135	0.0412	0.0013	260.0	± 8.6	256.8	± 13.6
50	0.77	0.0505	0.0015	0.2082	0.0061	0.0299	0.0007	189.7	± 4.7	192.1	± 6.2
51	0.51	0.0529	0.0018	0.3081	0.0110	0.0422	0.0012	266.7	± 7.6	272.7	± 11.1
52	0.58	0.0521	0.0012	0.2890	0.0072	0.0402	0.0009	254.2	± 6.1	257.7	± 7.3
53	0.42	0.0505	0.0012	0.2849	0.0069	0.0409	0.0010	258.3	± 6.1	254.6	± 7.0
54	0.62	0.0507	0.0030	0.2996	0.0188	0.0428	0.0017	270.3	± 11.1	266.1	± 18.9
55	0.47	0.0508	0.0014	0.2259	0.0062	0.0322	0.0008	204.6	± 5.0	206.8	± 6.3
57	0.67	0.0495	0.0013	0.2089	0.0054	0.0306	0.0007	194.1	± 4.6	192.6	± 5.4
58	0.09	0.0501	0.0012	0.2876	0.0071	0.0416	0.0010	262.6	± 6.3	256.6	± 7.2
59	0.67	0.0505	0.0011	0.2223	0.0047	0.0319	0.0007	202.6	± 4.5	203.8	± 4.8
60	0.60	0.0504	0.0014	0.2100	0.0061	0.0302	0.0007	191.7	± 4.7	193.6	± 6.2
61	0.75	0.0518	0.0020	0.3020	0.0123	0.0423	0.0013	266.9	± 8.1	268.0	± 12.4
62	0.86	0.0516	0.0015	0.2913	0.0087	0.0409	0.0010	258.3	± 6.7	259.6	± 8.8
Discordant data											
56	0.17	0.1103	0.0014	3.7336	0.0569	0.2453	0.0055	1414.4	± 35.2	1578.6	± 56.2
Standards											
91500 2-6	0.37	0.0745	0.0017	1.8184	0.0641	0.1769	0.00503	1050	± 32	1052	± 63
91500 2-7	0.39	0.0755	0.0018	1.8656	0.0657	0.1791	0.00510	1062	± 33	1069	± 65
91500 2-8	0.42	0.0746	0.0017	1.8679	0.0656	0.1814	0.00515	1075	± 33	1070	± 65
91500 3-1	0.39	0.0761	0.0016	1.8643	0.0536	0.1776	0.00533	1053.6	± 34.3	1068.5	± 53.0
91500 3-2	0.36	0.0764	0.0016	1.9173	0.0547	0.1818	0.00544	1076.7	± 35.0	1087.1	± 54.1
OD3 3-1	1.51	0.0485	0.0021	0.0352	0.0015	0.0053	0.00013	33.8	± 0.9	35.1	± 1.5
OD3 3-2	1.07	0.0484	0.0026	0.0345	0.0017	0.0052	0.00014	33.2	± 0.9	34.5	± 1.8
OD3 3-3	1.13	0.0475	0.0021	0.0332	0.0014	0.0051	0.00013	32.5	± 0.8	33.1	± 1.5

Table 2 Zircon U–Pb isotopic data for Sample Skm-08 obtained by quadrupole inductively coupled plasma mass spectrometry.

No.	Th/U	Isotopic ratios						U–Pb age (Ma)			
		$^{207}Pb/^{206}Pb$	Error 2σ	$^{207}Pb/^{235}U$	Error 2σ	$^{206}Pb/^{238}U$	Error 2σ	$^{206}Pb/^{238}U$	Error 2σ	$^{207}Pb/^{235}U$	Error 2σ
1	0.89	0.0515	0.0015	0.2868	0.0090	0.0404	0.0011	255.2	± 7.2	256.1	± 9.1
2	0.59	0.0515	0.0018	0.2888	0.0114	0.0407	0.0013	257.0	± 8.1	257.6	± 11.5
3	0.98	0.0519	0.0015	0.3068	0.0101	0.0428	0.0012	270.4	± 7.8	271.7	± 10.2
4	0.83	0.0518	0.0012	0.2908	0.0073	0.0407	0.0010	256.9	± 6.7	259.2	± 7.4
5	0.68	0.0555	0.0014	0.3025	0.0082	0.0395	0.0010	249.6	± 6.7	268.4	± 8.3
6	0.37	0.0506	0.0013	0.2669	0.0076	0.0382	0.0010	242.0	± 6.6	240.2	± 7.7
7	1.53	0.0515	0.0013	0.2862	0.0079	0.0403	0.0011	254.7	± 6.9	255.5	± 7.9
8	1.04	0.0517	0.0013	0.2901	0.0078	0.0406	0.0011	256.8	± 6.9	258.7	± 7.9
9	1.04	0.0507	0.0013	0.2751	0.0079	0.0393	0.0011	248.8	± 6.8	246.7	± 8.0
10	0.53	0.0520	0.0014	0.2900	0.0087	0.0404	0.0011	255.3	± 7.1	258.6	± 8.8
11	0.80	0.0521	0.0012	0.2943	0.0078	0.0409	0.0011	258.5	± 6.9	261.9	± 7.9
12	1.06	0.0535	0.0015	0.3014	0.0092	0.0408	0.0011	258.0	± 7.3	267.5	± 9.3
13	0.53	0.0523	0.0014	0.2577	0.0075	0.0357	0.0010	226.1	± 6.2	232.8	± 7.6
14	0.68	0.0523	0.0014	0.2966	0.0090	0.0411	0.0011	259.5	± 7.3	263.8	± 9.0
15	0.74	0.0514	0.0011	0.2727	0.0065	0.0385	0.0010	243.4	± 6.3	244.8	± 6.5
16	0.41	0.0713	0.0016	1.5394	0.0428	0.1565	0.0045	937.2	± 29.2	946.3	± 42.6
17	0.65	0.0546	0.0020	0.3796	0.0161	0.0504	0.0017	316.8	± 10.8	326.8	± 16.3
18	1.15	0.0509	0.0011	0.2454	0.0057	0.0349	0.0009	221.4	± 5.7	222.9	± 5.8
19	1.30	0.0521	0.0015	0.3111	0.0102	0.0433	0.0012	273.2	± 7.9	275.0	± 10.3
20	0.28	0.0525	0.0027	0.2971	0.0171	0.0410	0.0016	259.0	± 10.3	264.1	± 17.2
21	0.53	0.0507	0.0013	0.2831	0.0104	0.0404	0.0009	255.6	± 5.6	253.1	± 10.5
22	0.62	0.0511	0.0013	0.2968	0.0113	0.0421	0.0009	266.0	± 6.0	263.9	± 11.4
23	0.63	0.0503	0.0013	0.2807	0.0107	0.0405	0.0009	255.7	± 5.8	251.2	± 10.9
24	0.30	0.0513	0.0009	0.2685	0.0083	0.0380	0.0007	240.2	± 4.5	241.5	± 8.4
25	0.62	0.0521	0.0014	0.2907	0.0114	0.0404	0.0009	255.6	± 5.9	259.1	± 11.5
26	0.56	0.0517	0.0010	0.2869	0.0093	0.0402	0.0008	254.0	± 4.9	256.1	± 9.4
27	0.75	0.0519	0.0018	0.3001	0.0136	0.0419	0.0011	264.7	± 7.1	266.5	± 13.7
28	0.60	0.0503	0.0018	0.2765	0.0129	0.0399	0.0011	252.1	± 6.8	247.9	± 13.0
29	0.67	0.0518	0.0012	0.3067	0.0109	0.0429	0.0009	270.8	± 5.7	271.6	± 11.0
30	0.33	0.0502	0.0010	0.2874	0.0095	0.0415	0.0008	262.3	± 5.2	256.5	± 9.6
31	0.54	0.0537	0.0015	0.3067	0.0122	0.0414	0.0010	261.7	± 6.2	271.6	± 12.3
32	0.71	0.0508	0.0011	0.2945	0.0101	0.0420	0.0008	265.3	± 5.4	262.1	± 10.2
33	1.09	0.1656	0.0025	11.2670	0.3693	0.4931	0.0114	2584.1	± 72.9	2545.5	± 319.1
34	0.62	0.0510	0.0012	0.2928	0.0103	0.0416	0.0009	262.5	± 5.5	260.7	± 10.4
35	1.37	0.0520	0.0012	0.3129	0.0108	0.0436	0.0009	275.1	± 5.7	276.4	± 10.9
36	0.63	0.0570	0.0020	0.3278	0.0151	0.0417	0.0011	263.4	± 7.3	287.9	± 15.2

Continued.

Table 2 Continued.

No.	Th/U	Isotopic ratios						U–Pb age (Ma)			
		$^{207}Pb/^{206}Pb$	Error 2σ	$^{207}Pb/^{235}U$	Error 2σ	$^{206}Pb/^{238}U$	Error 2σ	$^{206}Pb/^{238}U$	Error 2σ	$^{207}Pb/^{235}U$	Error 2σ
37	0.15	0.1144	0.0017	5.3096	0.1630	0.3363	0.0067	1869.1	± 43.2	1870.4	± 153.3
38	0.58	0.0511	0.0009	0.2714	0.0083	0.0385	0.0007	243.3	± 4.5	243.8	± 8.4
39	0.67	0.0520	0.0011	0.2928	0.0097	0.0408	0.0008	257.9	± 5.1	260.8	± 9.8
40	0.63	0.0524	0.0012	0.2969	0.0103	0.0410	0.0008	259.2	± 5.4	263.9	± 10.4
41	0.67	0.0528	0.0014	0.3144	0.0103	0.0432	0.0009	272.4	± 5.9	277.6	± 10.4
42	0.84	0.0510	0.0010	0.2783	0.0076	0.0395	0.0007	250.0	± 4.7	249.3	± 7.7
43	0.61	0.0518	0.0011	0.2922	0.0079	0.0409	0.0008	258.5	± 4.8	260.3	± 8.0
44	0.64	0.0511	0.0012	0.2997	0.0090	0.0425	0.0008	268.2	± 5.4	266.2	± 9.1
45	0.12	0.0523	0.0008	0.3095	0.0071	0.0429	0.0007	270.8	± 4.6	273.8	± 7.1
46	0.78	0.0524	0.0011	0.3212	0.0093	0.0444	0.0009	280.1	± 5.5	282.8	± 9.4
47	0.57	0.0520	0.0019	0.2805	0.0120	0.0391	0.0010	247.1	± 6.5	251.0	± 12.1
48	0.42	0.1219	0.0015	6.0552	0.1458	0.3601	0.0074	1982.7	± 47.6	1983.8	± 138.2
49	0.40	0.0513	0.0009	0.2834	0.0069	0.0401	0.0007	253.2	± 4.4	253.3	± 7.0
50	0.67	0.0517	0.0009	0.2874	0.0072	0.0403	0.0007	254.5	± 4.5	256.5	± 7.3
51	0.78	0.0513	0.0008	0.2649	0.0061	0.0374	0.0006	236.7	± 3.9	238.6	± 6.1
52	0.63	0.0522	0.0011	0.2990	0.0083	0.0415	0.0008	262.2	± 5.0	265.6	± 8.4
53	0.46	0.0512	0.0018	0.3194	0.0134	0.0452	0.0012	285.2	± 7.6	281.5	± 13.5
54	0.69	0.0507	0.0010	0.2851	0.0074	0.0408	0.0007	257.6	± 4.7	254.7	± 7.4
55	0.68	0.0502	0.0018	0.3018	0.0131	0.0435	0.0012	274.8	± 7.4	267.8	± 13.3
56	0.88	0.0527	0.0011	0.3514	0.0099	0.0483	0.0009	304.2	± 6.0	305.7	± 10.0
57	0.72	0.0517	0.0011	0.2873	0.0079	0.0403	0.0007	254.7	± 4.8	256.4	± 7.9
58	0.17	0.1200	0.0014	5.7920	0.1245	0.3499	0.0062	1934.1	± 40.0	1945.2	± 119.2
59	0.60	0.0518	0.0014	0.2995	0.0100	0.0419	0.0009	264.9	± 5.8	266.0	± 10.1
60	0.39	0.0521	0.0017	0.3015	0.0119	0.0420	0.0010	265.0	± 6.6	267.6	± 12.0
Standards											
91500epo 4-1	0.41	0.0746	0.0016	1.8877	0.0637	0.1833	0.00560	1085	± 36	1077	± 63
91500epo 4-2	0.38	0.0745	0.0015	1.8759	0.0711	0.1826	0.00496	1081	± 32	1073	± 70
91500epo 4-3	0.38	0.0757	0.0013	1.8978	0.0591	0.1817	0.00469	1076	± 30	1080	± 58
OD3 4-1	1.09	0.0481	0.0017	0.0346	0.0013	0.0052	0.00012	33.5	± 0.8	34.5	± 1.4
OD3 4-2	1.16	0.0466	0.0012	0.0329	0.0012	0.0051	0.00009	32.9	± 0.6	32.9	± 1.2
OD3 4-3	1.30	0.0479	0.0017	0.0345	0.0013	0.0052	0.00009	33.5	± 0.6	34.4	± 1.3

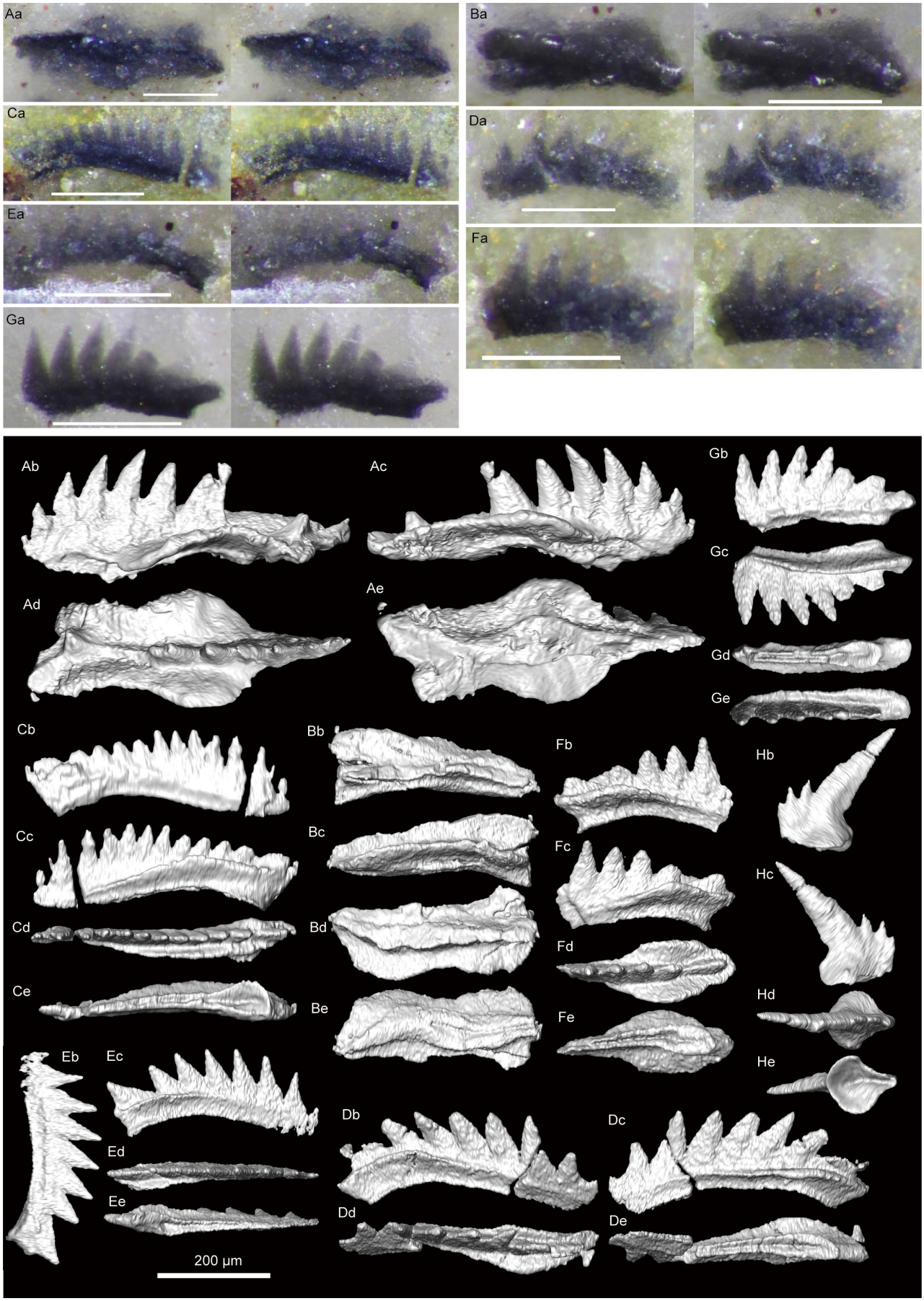
Aa
Ba
Ca
Da
Ea
Fa
Ga
Ab
Ac
Gb
Gc
Ad
Ae
Gd
Ge
Cb
Bb
Fb
Hb
Cc
Bc
Fc
Hc
Cd
Bd
Fd
Hd
Ce
Be
Fe
He
Eb
Ec
Db
Dc
Ed
Ee
Dd
De
200 µm

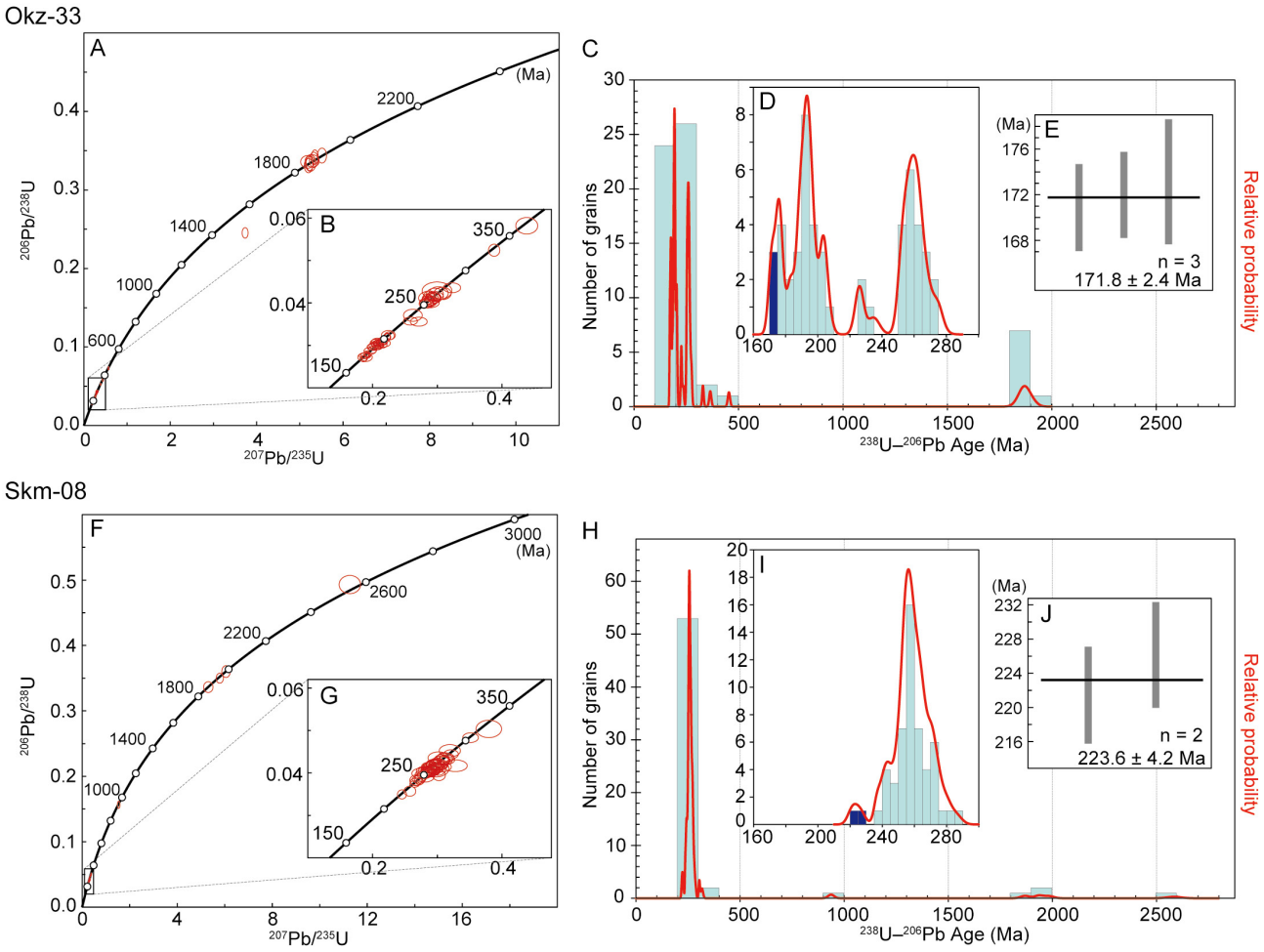

Fig. 12 (A, B, F, G) Concordia diagrams of zircon ages from sandstone. (A, B) Okz-33, Okoshi Stream. (A) All grains. (B) Phanerozoic grains. (F, G) Skm-08, Sakamoto. (F) All grains. (G) Phanerozoic grains. (C–E, H–J) Probability density plot and histogram of concordant zircon ages (C, D, H, I) and bar plots (E, J) of $^{206}Pb/^{238}U$ ages of the youngest cluster. The youngest cluster determined by overlaps of 1σ error (YC1σ) is shown with deep blue in the histograms. (C–E) Okz-33. n = 58; YC1σ (n = 3): 171.8 ± 2.4 Ma, MSWD = 0.24; Youngest single grain (YSG): 170.9 ± 3.8 Ma. (H–J) Skm-08. n = 59; YC1σ (n = 2): 223.6 ± 4.2 Ma, MSWD = 1.3; YSG: 221.4 ± 5.7 Ma. Figures were produced by Isoplot/Ex 4.15 (Ludwig, 2012).

5. Accretionary age of the Otori Unit

Previously, the accretionary age of the Otori Unit was constrained only by the late Bajocian to early Bathonian radiolarians from manganese nodules in siliceous mudstone (Suzuki *et al.*, 2007). The outcrop they investigated (Loc. S07 in Fig. 3) is an isolated one surrounded by mudstone outcrops, which led the authors to avoid making assumptions about which part of the oceanic plate stratigraphy the sample belongs to. In this study, we obtained Bathonian radiolarians from a manganese nodule within siliceous mudstone of the coherent Okoshizawa Subunit. The siliceous mudstone of the Okoshizawa Subunit is visibly different from mudstone matrix of mixed facies in that fragmented rock pieces and seams are absent (compare Figs. 7B, 9A, B). Hence, the radiolarians therein can be used an indicator of the time of deposition

(← p. 18)

Fig.11 Conodonts obtained from chert in the lowermost part of the Okoshizawa Subunit (Okz-CO-01). Figures with subscripts a are stereographic pairs (parallel viewing) of photographs and those with subscripts b through e are 3D-images obtained by X-ray computed microtomography for the same specimen. Subscripts b and c show lateral views, d shows upper views and e shows basal views. (A) *Sephardiella mungoensis*. (B) *S.* cf. *mungoensis*. (C–E) *Paragondolella* cf. *inclinata* (juvenile). (F) *Paragondolella polygnathiformis* (juvenile). (G) *Paragondolella* sp. (juvenile). (H) *Misikella longidentata*.

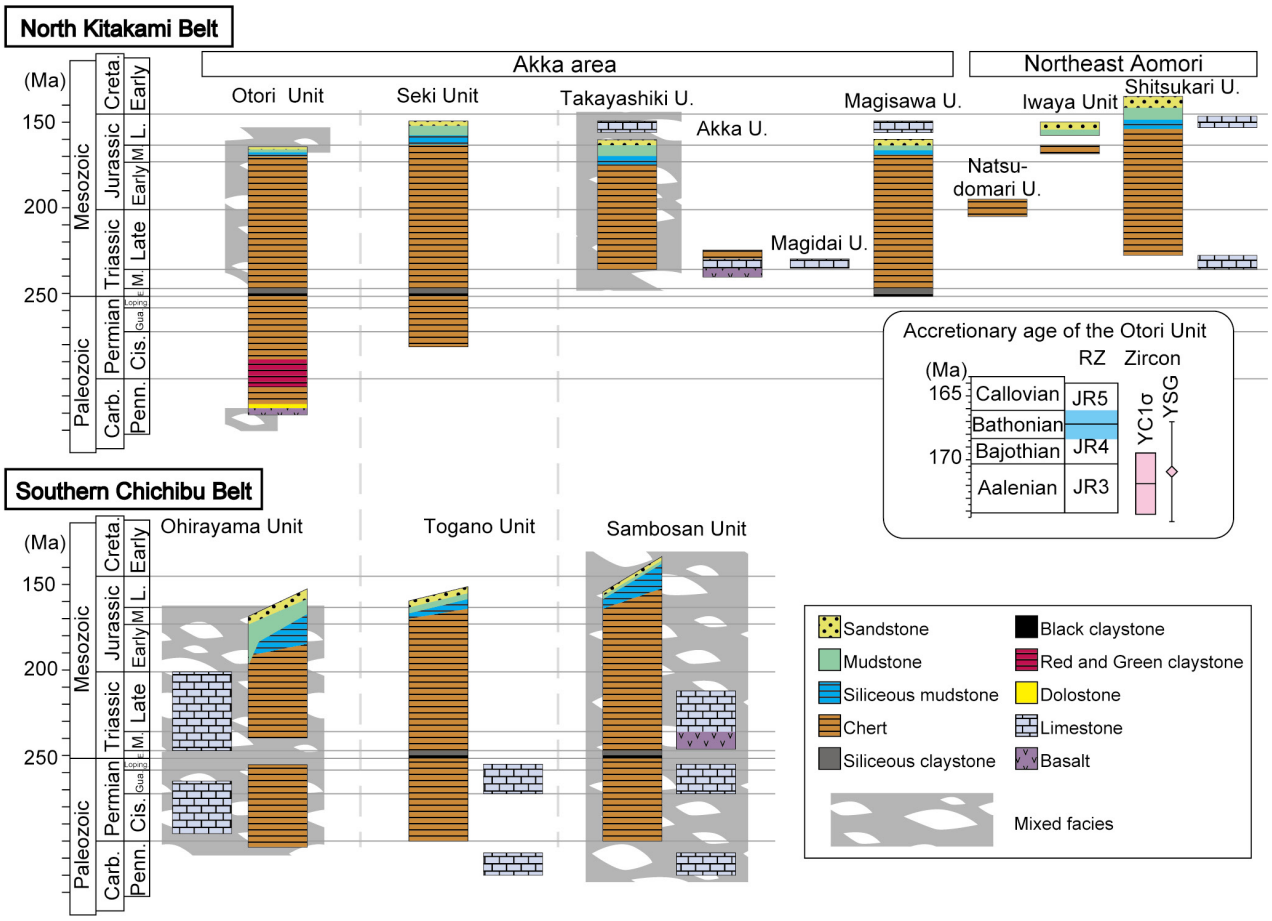

Fig. 13 Oceanic plate stratigraphy of the northeast part of the North Kitakami Belt (based on part of Fig. 7 of Uchino and Suzuki, 2020) and the Southern Chichibu Belt (Matsuoka *et al.*, 1998). U.: Unit; RZ: radiolarian zonation; Carb.: Carboniferous; Creta: Cretaceous; Penn.: Pennsylvanian; Cis.: Cisuralian; Gua.: Guadalupian; Loping.: Lopingian; E.: Early; M.: Middle; L.: Late.

of siliceous mudstone, and thus an approximation for the timing of accretion.

Detrital zircons of sample Okz-33 had a YC1σ of 171.8 ± 2.4 Ma and a YSG of 170.9 ± 3.8 Ma. Considering the occurrence of Bathonian radiolarians from the Otori Unit, it is expected that the depositional age of sandstone of this unit is Bathonian or younger. Therefore, the U–Pb age of Okz-33 is considered to be close to the accretionary age. The youngest zircon grains in sample Skm-08 were Late Triassic zircons, but there is no reason to assume that the two samples belong to different tectonostratigraphic units. In fact, the main components of detrital zircons in Skm-08, the Late Triassic grains, the overwhelmingly dominant Permian–Triassic grains and the Paleo-proterozoic grains, are also present in Okz-33, suggesting that they had a similar provenance (Fig. 12). Therefore, we interpret that Skm-08 and Okz-33 are both components of a middle Jurassic accretionary complex, and that the Late Triassic zircons in Skm-08 are zircons that crystallized long before transportation to the trench. A similar example of detrital zircon age trends from two closely located sandstones has been reported from the Middle Jurassic accretionary complex in the Okawa area, ~30 km southwest of our study area (Uchino, 2021). This implies that sandstones apparently lacking detrital zircon ages close to the depositional age may not be uncommon, at least in the Middle Jurassic accretionary complex of the North Kitakami Belt. Consequently, the accretionary age of the Otori Unit is estimated as the Bathonian.

6. Regional correlations

The North Kitakami Belt has been regarded as the northern extension of the Southern Chichibu Belt and correlations of their internal tectonostratigraphic divisions have been discussed (Yamakita and Otoh, 2000; Otoh and Sasaki, 2003; Ehiro *et al.*, 2008; Takahashi *et al.*, 2016). Presently available data is not sufficient to determine a correlative counterpart of the Otori Unit in the Southern Chichibu Belt. However, below is a comparison of the North Kitakami and Southern Chichibu belts incorporating our new information of lithology and age.

The most striking similarity between the North Kitakami Belt and the Southern Chichibu Belt is the occurrence of large (> km scale) Triassic basalt–limestone bodies in the structurally lower part (Fig. 13). Such massive Triassic basalt–limestone bodies are not seen in the Jurassic accretionary complex of the Tamba–Mino–Ashio Belt in the inner zone of Southwest Japan (e.g., Nakae, 2000). In the North Kitakami Belt, the basalt–limestone bodies are represented by the Akka Unit (Yoshida *et al.*, 1987; Toyohara *et al.*, 1980) and Triassic limestone in Shiriya, northeast Aomori (Sano *et al.*, 2009). In the Southern Chichibu Belt, the Triassic basalt–limestone bodies characterize the Sambosan Unit (Matsuoka *et al.*, 1998). In both the North Kitakami and Southern Chichibu belts, the unit including the basalt–limestone bodies are structurally overlain by a tectonostratigraphic unit composed of coherent chert–clastic sequences; the Seki Unit in the former and the Togano Unit in the latter (Otoh and Sasaki, 2003; Takahashi *et al.*, 2016).

The Otori Unit structurally overlies the Seki Unit. Based on this, the Otori Unit was correlated with the Ohirayama Unit, which structurally overlies the Togano Unit in the Southern Chichibu Belt (Otoh and Sasaki, 2003; Takahashi *et al.*, 2016). Takahashi *et al.* (2016) also argued that the occurrence of Carboniferous to Triassic chert was an important similarity. Previous studies regarded the Otori Unit as a coherent facies of chert and mudstone (Ehiro *et al.*, 2008; Takahashi *et al.*, 2016), while the Ohirayama Unit is characterized by a mixed facies including blocks of Permian limestone, sandstone and chert (Matsuoka *et al.*, 1998). This difference was an unexplained issue in Takahashi *et al.* (2016), but our geological survey clarified that a large part of the Otori Unit is composed of mixed facies rather than coherent facies. Thus, the mixed facies is another similarity between the Otori and Ohirayama units. However, a significant difference in lithology remains between the two: Permian limestone blocks that are characteristic of the Ohirayama Unit is completely absent in the Otori Unit.

Regarding the accretionary age of the Ohirayama Unit, Matsuoka *et al.* (1998) summarized radiolarian fossil occurrences mainly in Shikoku and regarded the age of mudstone of this unit as Pliensbachian to Toarcian. Later reports of radiolarians from correlative units in west Kyushu are consistent, indicating a Sinemurian to early Toarcian age for mudstone (Saito *et al.*, 2005). In the Kii Peninsula, radiolarians from mudstone indicate a wider age range from the Pliensbachian to Kimmeridgian (Yamato Omine Research Group, 1992, 2002, 2005, 2007, Kashiwagi *et al.*, 2005). The U–Pb age of detrital zircons in the Kii Peninsula is consistent with the radiolarian-based age (Tokiwa *et al.*, 2019). In the Kanto Mountains, radiolarians indicate a Pliensbachian to Bathonian age for siliceous mudstone and a Hettangian to Bathonian age (mostly Aalenian to Bathonian) for mudstone (Hisada and Kishida, 1986; Hisada *et al.*, 1992; Takahashi, 2000; Yoshida and Matsuoka, 2003; Matsuoka, 2011; Ito and Matsuoka, 2018). The accretionary age of the Otori Unit is within the range of accretionary age of the Ohirayama Unit in the Kii Penisnsula and Kanto Mountains (Fig. 13). However, the age of siliceous mudstone is significantly older in the Ohirayama Unit in some regions, resulting in the apparently longer age range for mudstone in the Ohirayama Unit (Fig. 13). However, it should be noted that the age of siliceous mudstone in the Otori Unit is controlled only by a few samples and its entire age range may be longer.

To summarize, the Otori Unit has the same tectonostratigraphic position and mixed facies as the Ohirayama Unit, while they differ in that the Otori Unit lacks limestone blocks and appears to have a younger age of siliceous mudstone. Matsuoka *et al.* (1998) noted that the distribution of the Ohirayama Unit in the type locality in Shikoku is much narrower compared to areas such as the Kanto Mountains and suggested that a part of the Jurassic accretionary complex of the Southern Chichibu Belt in the Kanto Mountains may be lacking in Shikoku. Similarly, the correlative counterpart of the Otori Unit may not be present in the type locality of the Ohirayama Unit, which could explain the discrepancies between the two units.

7. Conclusions

We investigated the lithology, structure and accretionary age of the Otori Unit, distributed in the northeastern part of the North Kitakami Belt. The Otori Unit is composed of two subunits: the structurally lower Okoshizawa Subunit composed of coherent facies of chert and siliceous mudstone and the structurally upper Osakamoto Subunit composed of mixed facies of mudstone, sandstone, chert and minor basaltic rocks. A manganese nodule in the siliceous mudstone of the Okoshizawa Subunit yielded radiolarians indicating the upper JR4 to lower JR5 biozone (Bathonian, Middle Jurassic). Radiolarians from siliceous mudstone of both the Okoshizawa and Osakamoto subunits can be interpreted to be of the same age. Detrital zircon grains from sandstone in the Osakamoto Subunit has a youngest age of ~170 Ma (YC1σ: 171.8 ± 2.4 Ma; YSG: 170.9 ± 3.8 Ma). Based on the radiolarian and detrital zircon ages, the accretionary age of the Otori Unit is estimated as the Bathonian. The Otori Unit has formerly been compared with the Ohirayama Unit of the Southern Chichibu Belt, but there are significant differences in the lithofacies and age of the two.

8. Palaeontological notes

Conodonts (by MUTO Shun)

Misikella longidentata Kozur and Mock
(Fig. 11H)

1974 *Misikella longidentata* — Kozur and Mock, p. 136–137, pl. 1, figs. 4, 5.

Remarks: This species is distinguished by a short segminate element with a terminal, posteriorly curved cusp more than twice as high (measured from the base of element) and thick as the other denticles, which decrease size away from the cusp. The basal cavity is laterally expanded.

Paragondolella* cf. *inclinata (Kovács)
(Fig. 11C, D, E)
1983 *Gondolella foliata inclinata* — Kovács, p. 110–111, pl. 1, figs. 1–4, pl. 3, figs. 2–4.
Remarks: Juvenile forms of this species possess a narrow platform forming in the posterior part of the element. In our specimens, the denticles gradually recline and decrease height in the posterior to a thick terminal cusp. Our specimens are most likely to be assigned to this species. *Paragondolella bulgarica* (Budurov & Stefanov) is similar but has a uniformly high carina. Detailed synonymy is given by Chen and Lukeneder (2017).

Paragondolella polygnathiformis (Budurov and Stefanov)
(Fig. 11F)
1965 *Gondolella polygnathiformis* — Budurov and Stefanov, p. 118–119, pl. 3, figs. 3–7.
Remarks: Ontogenetic development of this species is clearly demonstrated by Koike (1982, 1991). From the early stages, like our specimen, it has a platform with a constriction beside the cusp running almost to the anterior end and a geniculation point at mid-length where the platform margin steps down towards the anterior in lateral view. Detailed synonymy is given by Chen and Lukeneder (2017).

Sephardiella mungoensis (Diebel)
(Fig. 11A)
Sephardiella* cf. *mungoensis (Diebel)
(Fig. 11B)
1956 *Polygnathus mungoensis* — Diebel, p. 431–432, pl. 1, figs. 1–20, pl. 2, figs. 1–4, pl. 3, fig. 1, pl. 4, fig. 1.
Remarks: This species is distinguished by a free blade, a sinuous platform with ornamentations on the lateral edge and a well-developed posterior process. The specimen in Fig. 11B is rather poorly imaged and broken at the anterior, but the platform outline and posteriorly extended keel matches the characters of *S. mungoensis*.
Plasencia *et al.* (2007, 2018) argued that the genus name *Sephardiella* proposed by March *et al.* (1988) and described by March *et al.* (1990) has priority over the more commonly used *Budurovignathus*, which was established without diagnosis or description by Kozur (1988). Both *Sephardiella* (March *et al.*, 1988) and *Budurovignathus* (Kozur, 1988) were proposed as replacement names for *Carinella* Budurov. According to ICZN Article 13.1.1 to 13.1.3, new names are required to be accompanied by a description or definition, or by bibliographic reference to such a statement, or to be proposed as a new replacement name. The third case applies to both *Sephardiella* (March *et al.*, 1988) and *Budurovignathus* (Kozur, 1988), and thus both are available and have equal priority, contrary to the statements in Plasencia *et al.* (2018). However, as Plasencia *et al.* (2007) mentioned, Sudar (1989) selected *Sephardiella* as the first reviser six months prior to Kozur (1989) that preferred *Budurovignathus*, and the former is the valid name.

Radiolarians (by ITO Tsuyoshi)

Order **NASSELLARIA** Ehrenberg, 1875
Family **DIACANTHOCAPSIDAE** O'Dogherty, 1994
Genus ***Diacanthocapsa*** Squinabol, 1903
Type species ***Diacanthocapsa euganea*** Squinabol, 1903

Diacanthocapsa*? *operculi Yao
(Plate 1, fig. 5)
1979 *Diacanthocapsa*? *operculi* — Yao, pl. 2, figs. 16–27
Remarks: The specimen has a fusiform shell with four segments. The segmentation is closely similar to the species (Yao, 1979).

Subfamily **JAPONOCAPSINAE** Kozur, 1984
Genus ***Japonocapsa*** Kozur, 1984
Type species ***Tricolocapsa*? *fusiformis*** Yao, 1979

Japonocapsa fusiformis (Yao)
(Plate 1, fig. 1)
1979 *Tricolocapsa fusiformis* — Yao, p. 33, pl. 4, figs. 12–18, pl. 5, figs. 1–4.
1984 *Japonocapsa fusiformis* (Yao) — Kozur, 1984, p. 33, Plate 7, Fig. 2.
Remarks: The specimen has a fusiform shell with four segments. The fourth segment is dish-like and possesses large pores. These characteristics are closely similar with the species (Yao, 1979).

Japonocapsa* cf. *fusiformis (Yao)
(Plate 4, fig. 5; Plate 5, fig. 1)
Remarks: The specimens possess the large fourth segment. The outline of the shell is similar to *Japonocapsa fusiformis*, although the preservation is poor.

Genus ***Striatojaponocapsa*** Kozur, 1984
Type species ***Tricolocapsa plicarum*** Yao, 1979

Striatojaponocapsa synconexa O'Dogherty *et al.*, 2006.
(Plate 1, fig. 6; Plate 4, fig. 1)
2006 *Striatojaponocapsa synconexa* — O'Dogherty *et al.*, pl. 10, figs. 9–17.
Remarks: The specimens possess a small basal appendage with a circular porous depression. They closely resemble the species (O'Dogherty *et al.*, 2006; Hatakeda *et al.*, 2007).

Family **WILLIRIEDELLIDAE** Dumitrica, 1970
Genus ***Praezhamoidellum*** Kozur, 1984
Type species ***Praezhamoidellum yaoi*** Kozur, 1984

Praezhamoidellum*? cf. *japonicum (Yao)
(Plate 5, fig. 2)

1979 *Stichocapsa japonica* Yao, 1979, Plate 6, figs. 8–12.

Remarks: The specimen has a truncate–conical thorax–abdomen with a flat base. Large opening is recognized in the basal part. These characteristics are similar to *Praezhamoidellum*? *japonicum* (Yao, 1979).

Family **Unumidae** Kozur, 1984
Genus ***Protunuma*** Ichikawa and Yao, 1976
Type species ***Protunuma fusiformis*** Ichikawa and Yao, 1976

Protunuma fusiformis Ichikawa and Yao
(Plate 1, fig. 3)

1976 *Protunuma fusiformis* Ichikawa and Yao, pl. 2, figs. 1–4.

Remarks: The specimen has a fusiform shell composed of multi-segments. No spine is observed on the surface, but circular pores aligned in longitudinal rows are recognized. These characteristics are closely similar to the species (Yao, 1979).

Family **Gongylothoracidae** Bak, 1999
Genus ***Gongylothorax*** Foreman, 1968
Type species ***Dicolocapsa verbeeki*** Tan Sin Hok, 1927

Gongylothorax siphonofer Dumitrica
(Plate 1, fig. 2)

1970 *Gongylothorax siphonofer* — Dumitrica, pl. 1, figs. 2–5.

Remarks: The specimen has a sub-spherical shell of two segments. The shell outline and inner structure is closely similar to the species reported from Japan (Yao, 1979).

Family **EUCYRTIDIELLIDAE** Takemura, 1986
Genus ***Eucyrtidiellum*** Baumgartner, 1984
Type species ***Eucyrtidium*? *unumaensis*** Yao, 1979

Eucyrtidiellum unumaense (Yao, 1979)
(Plate 1, figs. 7, 8)

1979 ***Eucyrtidium*? *unumaensis*** — Yao, pl. 9, figs. 1–11.

1984 *Eucyrtidiellum unumaensis* (Yao) — Baumgartner, pl. 4, fig. 6.

Remarks: The specimens have a small cephalis with apical horn and truncate-conical thorax. They closely resemble the species (Yao, 1979).

Acknowledgements

The manuscript benefited from attentive comments from Uchino T. and Nagamori H. We are sincerely grateful to Yagyu, S. for operating the X-ray microscope at Kochi University. The authors thank Iwano, H. and Danhara, T. of Kyoto Fission-Track Co. Ltd. For extraction and analysis of detrital zircons. We are grateful to Suzuki, N. of the Tohoku University for sharing information about the treatment of manganese nodules, to Dr. S. Takahashi for providing us the illustrations of Ehiro *et al.* (2008) and to Shimura, Y. of the Geological Survey of Japan and Danhara, Y. of Kyoto Fission-Track Co. Ltd. For teaching us the analytical procedures of Isoplot 4.15.

References

Bak, M. (1999) Uppermost Maastrichtian Radiolaria from the Magura Nappe deposits, Czech Outer Carpathians. *Annales Societatis Geologorum Poloniae*, **69**, 137–159.

Baumgartner, P. O. (1984) A Middle Jurassic–Early Cretaceous low latitude radiolarian zonation based on unitary associations and age of Tethyan radiolarites. *Eclogae Geologicae Helvetiae*, **77**, 729–841.

Budurov, K. and Stefanov, S. (1965) Gattung Gondolella aus der Trias Bulgariens. *Trudove Byrkhu Geologiyata na Bylgariya, Seriya Paleontologiya [Traveaux Géologiques de Bulagrie Série Paléontologie]*, **7**, 115–121. (in German)

Chen, Y. and Lukeneder, A. (2017) Late Triassic (Julian) conodont biostratigraphy of a transition from reefal limestones to deep-water environments on the Cimmerian terranes (Taurus Mountains, southern Turkey). *Papers in Palaeontology*, **3**, 441–460.

Chen, Y., Krystyn, L., Orchard, M. J., Lai, X. L. and Richoz, S. (2016) A review of the evolution, biostratigraphy, provincialism and diversity of Middle and early Late Triassic conodonts. *Papers in Palaeontology*, **2**, 235–263.

Dickinson, W. R. and Gehrels, G. E. (2009) Use of U-Pb ages of detrital zircons to infer maximum depositional ages of strata: A test against a Colorado Plateau Mesozoic database. *Earth and Planetary Science Letters*, **288**, 115–125.

Diebel, K. (1956) Conodonten in der Ober Kreide von Kamerun. *Geologie*, **5**, 424–450. (in German)

Dumitrica, P. (1970) Cryptocephalic and cryptothoracic Nassellaria in some Mesozoic deposits of Romania. *Revue roumaine de Géologie, Géophysique et Géographie (série Géologie)*, **14**, 45–124.

Ehiro, M., Kawamura, M. and Kawamura, T. (2005) 1.1 Summary and Tectonostratigraphic divisions. *In* The Publishing Committee of the Geology of Japan, ed., *The Geology of Japan*. The Supplement. 49–50. (in Japanese)

Ehiro, M., Yamakita, S., Takahashi, S. and Suzuki, N. (2008) Jurassic accretionary complexes of the North Kitakami Belt in the Akka-Kuji area. *The Journal of the Geological Society of Japan*, **114** (Supplement), 121–139. (in Japanese)

Ehiro, M., Suzuki, N., Takahashi, S. and Yamakita, S.

(2017) 4.4 North Kitakami Belt. *In* The Geological Society of Japan ed., *Tohoku District*. 244–260.

Ehrenberg, C. G. (1875) *Fortsetzung der mikrogeologischen Studien als Gesammt-Uebersichtder mikroskopischen Palaontologie gleichartig analysirter Gebirgsarten der Erde, mit specieller Rucksicht auf den Polycystinen-Mergel von Barbados*. Abhandlungen der königlichen preussischen Akademie der Wissenschaften zu Berlin, 1–225. (in German)

Foreman, H. P. (1968) Upper Maestrichtian Radiolaria of California. *Special Papers in Palaeontology*, no. 3, 1–82.

Geological Survey of Japan, AIST (2020) Seamless digital geological map of Japan 1: 200,000. Geological Survey of Japan, AIST. https:// gbank.gsj.jp/seamless/ v2full/ (Accessed: 2021-10-08)

Hatakeda, K., Suzuki, N. and Matsuoka, A. (2007) Quantitative morphological analyses and evolutionary history of the Middle Jurassic polycystine radiolarian genus Striatojaponocapsa Kozur. *Marine Micropaleontology*, **63**, 39–56.

Hirata, T., Iizuka, T. and Orihashi, Y. (2005) Reduction of mercury background on ICP-mass spectrometry for in situ U–Pb age determinations of zircon samples. *Journal of Analytical Atomic Spectrometry*, **20**, 696–701.

Hisada, K., Ueno, H. and Igo, H. (1992) Geology of the Upper Paleozoic and Mesozoic sedimentary complex of the Mt. Ryokami area in the Kanto Mountains, central Japan. *Science reports of the Institute of Geoscience, University of Tsukuba, Section B, Geological sciences*, **13**, 127–151.

Hisada, K. and Kishida, Y. (1986) The Hamadaira Group in the western Kanto Mountains, central Japan—the developmental process of the Jurassic–lower Cretaceous accretionary prism—. *The Journal of the Geological Society of Japan*, **92**, 569–590. (in Japanese with English abstract)

Ichikawa, K. and Yao, A. (1976) Two new genera of Mesozoic cyrtoid radiolarians from Japan. *In* Takayanagi, Y. and Saito, T., eds. *Progress in Micropaleontology*, *Special Publication*, Micropaleontology Press, The American Museum of Natural History, New York, 110–117.

Iizuka, T. and Hirata, T. (2004) Simultaneous determinations of U–Pb age and REE abundances for zircons using ArF excimer laser ablation-ICPMS. *Geochemical Journal*, **38**, 229–241.

Isozaki, Y., Maruyama, S., Aoki, K., Nakama, T., Miyashita, A. and Otoh, S. (2010) Geotectonic subdivision of the Japanese Islands revisited: categorization and definition of elements and boundaries of Pacific-type (Miyashiro-type) orogen. *Chigaku Zasshi (Jounal of Geography)*, **119**, 999–1053. doi:10.5026/ jgeography.119.235 (in Japanese with English abstract)

Ito, T. and Matsuoka, A. (2018) Lithology and radiolarian age of the Ryokami-yama Chert Formation in eastern Mt. Ryokami: Possible décollement zone in Permian pelagic sequence in mid-Mesozoic accretionary complexes of Southwest Japan. *Island Arc*, **27**, e12273.

Iwano, H., Orihashi, Y., Hirata, T., Ogasawara, M., Danhara, T., Horie, K., Hasebe, N., Sueoka, S., Tamura, A., Hayasaka, Y., Katsube, A., Ito, H., Tani, K., Kimura, J., Chang, Q., Kouchi, Y., Haruta, Y. and Yamamoto, K. (2013) An inter-laboratory evaluation of OD-3 zircon for use as a secondary U–Pb dating standard. *Island Arc*, **22**, 382–394.

Kashiwagi, K., Niwa, M. and Tokiwa, T. (2005) Early Jurassic radiolarians from the Chichibu Composite Belt in the Sannokou area, central Kii Peninsula, Southwest Japan. *The Journal of the Geological Society of Japan*, **111**, 170–181.

Koike, T. (1982) Review of some platform conodonts of the Middle and Late Triassic in Japan. *Science reports of the Yokohama National University. Section II, Biological and geological sciences*, **29**, 15–27.

Koike, T. (1991) Triassic conodonts from exotic blocks of limestone in northern Kuzuu, the Ashio Mountains. *Science reports of the Yokohama National University. Section II, Biological and geological sciences*, **38**, 53–69.

Kojima, S., Hayasaka, Y., Hiroi, Y., Matsuoka, A., Sano, H., Sugamori, Y., Suzuki, N., Takemura, S., Tsujimori, T. and Uchino, T. (2016) 2b Pre-Cretaceous accretionary complexes. *In* Moreno, T., Wallis, S., Kojima, T. and Gibbons, W. eds., *The Geology of Japan*. Geological Society of London, London, 61–100.

Kovács, S. (1983) On the evolution of excelsa-stock in the upper Ladinian–Carnian (Conodonts, genus Gondolella, Triassic). *Schriftenreihe der erdwissenschaftlichen Kommission – Osterreichische Akademie der Wissenschaften*, **5**, 107–120.

Kozur, H. W. (1984) New radiolarian taxa from the Triassic and Jurassic. *Geologisch Paläontologische Mitteilungen Innsbruck*, **13**, 49–88.

Kozur, H. W. (1988) Division of the gondolellid platform conodonts. *In*: Ziegler, W. ed., *1st International Senckenberg Conference and 5th European Conodont Symposium (ECOS V). Part 2: Abstracts of Meeting*, Forschungsinstitut Senckenberg, Frankfurt, 244–245.

Kozur, H. W. (1989) The taxonomy of the gondolellid conodonts in the Permian and Triassic. *1st international Senckenberg conference and 5th European conodont symposium (ECOS V); Contribution III, Papers on Ordovician to Triassic conodonts*, **117**, 409–469.

Kozur, H. W. and Mock, R. (1974) Zwei neue Conodonten-Arten aus der Trias des Slowakischen Karstes. *Casopis pro Mineralogii a Geologii*, 135–139. (in German)

Ludwig, K. R. (2012) User's Manual for Isoplot 3.70: Geochronological Toolkit for Microsoft Excel. *Berkeley Geochronological Center Special Publication*, **5**, 1–75.

March, M., Budurov, K., Hirsch, F. and Marquez-Aliaga,

A. (1988) *Sephardiella* nov. gen (Conodonta), emendation of *Carinella* (Budurov, 1973), Ladinian (Middle Triassic). *In*: Ziegler, W. ed., *1st International Senckenberg Conference and 5th European Conodont Symposium (ECOS V). Part 2: Abstracts of Meeting*, Forschungsinstitut Senckenberg, Frankfurt, 247.

March, M., Budurov, K. and Hirsch, F. (1990) *Sephardiella* nov. gen. (Conodonta), emendation of *Carinella* (Budurov, 1973) from the Ladinian (Middle Triassic) type area in Catalonia (N. E. Spain), Sephardic Province. Papers on conodonts and Ordovician to Triassic conodont stratigraphy. *1st International Senckenberg Conference and 5th European Conodont Symposium (ECOS V), Contributions IV,* **118**, 197–202.

Matsuoka, A. (1987) Radiolarian age of the Shiriya Group in Aomori Prefecture, northeast Japan. *Fossils*, no. 42, 7–13. (in Japanese with English abstract)

Matsuoka, A. (1995) Jurassic and Lower Cretaceous radiolarian zonation in Japan and in the western Pacific. *Island Arc*, **4**, 140–153.

Matsuoka, A. and Ito, T. (2019) Updated radiolarian zonation for the Jurassic in Japan and the western Pacific. *Science reports of Niigata University (Geology)*, no. 34, 49–57.

Matsuoka, A. and Oji, T. (1990) Middle Jurassic radiolarian fossils from the Magisawa Formation in the Taro Belt, North Kitakami Mountains. *The Journal of the Geological Society of Japan,* **96**, 239–241. (in Japanese)

Matsuoka, A., Yamakita, S., Sakakibara, M. and Hisada, K. (1998) Unit division for the Chichibu Composite Belt from a view point of accretionary tectonics and geology of western Shikoku, Japan. *The Journal of the Geological Society of Japan*, **104**, 634–653. (in Japanese with English abstract)

Matsuoka, K. (2011) The radiolarians of the Ryokami Unit of the Southern Chichibu Belt in Otaki of Chichibu City, Saitama Prefecture, central Japan. *Bulletin of the Saitama Museum of Natural History New series*, **5**, 111–114. (in Japanese)

Minato, M. (1950) The geology of the Kitakami Mountains (Part 2). *Monograph of the Association for Geological Collaboration in Japan*, **5**, 1–28. (in Japanese)*

Minoura, K. (1985) Where did the Kitakami and Abukuma massifs come from?—the genesis of the geological structure of Northeast Japan—. *Kagaku*, **55**, 14–23. (in Japanese)*

Minoura, K. and Tsushima, M. (1984) Geology of the Omoto district in the eastern margin of the North Kitakami Massif. *Science reports of the Hirosaki University*, **31**, 93–107.

Murai, T., Okami, K. and Kudo, H. (1981) *Report on Silica Stone Resources of Iwate Prefecture for the 1980 Fiscal Year*. The Commerce, Industry, and Labor Relations Division of Iwate Prefecture, 13p. (in Japanese)

Murai, T., Okami, K. and Kudo, H. (1983) *Report on Silica Stone Resources of Iwate Prefecture for the 1982 Fiscal Year*. The Commerce, Industry, and Labor Relations Division of Iwate Prefecture, 43p. (in Japanese)

Muto, S., Takahashi, S., Yamakita, S., Suzuki, N., Suzuki, N. and Aita, Y. (2018) High sediment input and possible oceanic anoxia in the pelagic Panthalassa during the latest Olenekian and early Anisian: Insights from a new deep-sea section in Ogama, Tochigi, Japan. *Palaeogeography, Palaeoclimatology, Palaeoecology*, **490**, 687–707.

Muto, S., Yagyu, S., Takahashi, S. and Murayama, M. (2021) Identification of conodont fossils in pelagic deep-sea siliceous sedimentary rocks using laboratory-based X-ray computed microtomography. *Lethaia*, **54**, 687–699.

Nakae, S. (2000) Regional correlation of the Jurassic accretionary complex in the Inner Zone of Southwest Japan. *The Memoirs of the Geological Society of Japan*, no. 55, 73–98. (in Japanese with English abstract)

Nakae, S. and Kamada, K. (2003) Late Jurassic radiolarians from the Rikuchu-Seki district in the North Kitakami Belt, Northeast Japan. *The Journal of the Geological Society of Japan*, **109**, 722–725. (in Japanese with English abstract)

Nakae, S., Kamada, K., Kubo, K. and Kudo, T. (2021) *Geology of the Rikuchu Seki District*. Quadrangle Series, 1:50,000, Geological Survey of Japan, AIST. (in Japanese with English abstract)

O'Dogherty, L. (1994) Biochronology and paleontology of mid-Cretaceous radiolarians from Northern Apennines (Italy) and Betic Cordillera (Spain). *Mémoires de Géologie (Lausanne)*, **21**, 1–415.

O'Dogherty, L., Bill, S., Goričan, Š., Dumitrica, P. and Masson, H. (2006) Bathonian radiolarians from an ophiolitic mélange of the Alpine Tethys (Gets Nappe, Swiss-French Alps). *Micropaleontology*, **51**, 425–485.

O'Dogherty, L., Goričan, Š. and Gawlick, H. J. (2017) Middle and Late Jurassic radiolarians from the Neotethys suture in the Eastern Alps. *Journal of Paleontology*, **91**, 25–72.

Okami, K. and Ehiro, M. (1988) Review and recent progress of studies on the Pre-Miyakoan sedimentary rocks of the Northern Kitakami Massif, Northeast Japan. *Earth Science (Chikyu Kagaku)*, **42**, 187–201. (in Japanese with English abstract)

Onuki, Y. (1956) Geology of the Kitakami Mountains. *In* IwatePrefecture (ed.) *Explanatory Notes on the Geology of Iwate Prefecture*. *Part 2*. 1–189. (in Japanese)

Otoh, S. and Sasaki, M. (2003) Tectonostratigraphic division and regional correlation of the sedimentary complex of the North Kitakjami Belt. *Journal of Geography*, **112**, 406–410. (in Japanese)

Plasencia, P., Hirsch, F. and Márquez-Aliaga, A. (2007) Sephardiellinae, a new Middle Triassic conodont subfamily. *Journal of Iberian Geology*, **33**, 163–172.

Plasencia, P., Kiliç, A.M., Baud, A., Sudar, M. and Hirsch, F. (2018) The evolutionary trend of platform denticulation in middle triassic acuminate gondolellidae (Conodonta). *Turkish Journal of Zoology*, **42**, 187–197.

Saito, M., Miyazaki, K., Toshimitsu, S. and Hoshizumi, H. (2005) *Geology of the Tomochi District*. Quadrangle Series, 1:50,000, Geological Survey of Japan, AIST, 218p. (in Japanese with English abstract)

Sano, S., Sugisawa, N. and Shimaguchi, T. (2009) Discovery of megalodontoid bivalves in the Shiriya area, northern Honshu, northeast Japan, and its geological implications. *Memoir of the Fukui Prefectural Dinosaur Museum*, no. 8, 51–57. (in Japanese)

Shimazu, M., Tanaka, K. and Yoshida, T. (1970) *Geology of the Taro District*. Quadrangle Series, 1:50,000, Geological Survey of Japan, Kawasaki, 54p.

Sláma, J., Košler, J., Condon, D. J., Crowler, J. L., Gerdes, A., Hanchar, J. M., Horstwood, M. S. A., Morris, G. A., Nasdala, L., Norberg, N., Schaltegger, U., Schoene, B., Tubrett, M. N. and Whitehouse, M. J. (2008) Plešovice zircon - A new natural reference material for U–Pb and Hf isotopic microanalysis. *Chemical Geology*, **249**, 1–35.

Squinabol, S. (1903) Le Radiolarie dei noduli selciosi nella Scaglia degli Euganei. Contribuzione I. *Rivista Italiana di Paleontologia*, **9**, 105–151.

Sudar, M. (1989) Revision of conodont genera Sephardiella March, Budurov, Hisch & Marquez-Aiiaga, 1988, and *Budurovignathus* Kozur, 1988. *Geologica Balcanica*, **9**, 1989.

Sugimoto, M. (1969) Geology of the Omoto-Tanohata District, Outer Kitakami Belt, Northeast Japan. *Tohoku University, Institute of Geology and Paleontology Contributions*, **70**, 1–22. (in Japanese with English abstract)

Sugimoto, M. (1974) Stratigraphical study in the outer belt of the Kitakami Miassif, Northeast Japan. T*ohoku University, Institute of Geology and Paleontology Contributions*, **74**, 1–48. (in Japanese with English abstract)

Sugimoto, M. (1980) Geological structure (outline) of the Akka-Iwaizumi area, Northern Kitakami Mountains. *In*: Kimura, T. ed., *Report on the Multidiscipline Reseach Project A with 1979 Foundation of Grant-in-Aid for Scientific Research by the Education Ministry of Japan*, Tokyo Print Insatsu, Ltd., Tokyo 37–44. (in Japanese)*

Suzuki, N. and Ogane, K. (2004) Paleoceanographic affinities of radiolarian faunas in late Aalenian time (Middle Jurassic) recorded in the Jurassic accretionary complex of Japan. *Journal of Asian Earth Sciences,* **23**, 343–357.

Suzuki, N., Yamakita, S., Takahashi, S. and Ehiro, M. (2007) Middle Jurassic radiolarians from carbonate manganese nodules in the Otori Formation in the eastern part of the Kuzumaki-Kamaishi Subbelt, the North Kitakami Belt, Northeast Japan. *The Journal of the Geological Society of Japan*, **113**, 274–277. doi:10.5575/geosoc.113.274 (in Japanese with English abstract)

Tahahashi, O. (2000) Tectonostratigraphic study of the Chichibu and Shimanto Belts in the Kanto Mountains, central Japan. *The Journal of the Geological Society of Japan*, **106**, 836–852.

Takahashi, S., Ehiro, M., Suzuki, N. and Yamakita, S. (2016) Subdivisional scheme of the North Kitakami Belt, Northeast Japan and its tectonostratigraphic correlation to the Oshima and South Chichibu belts: an examination of the Jurassic accretionary complex in the west Akka area. *Journal of the Geological Society of Japan*, **122**, 1–22. doi:10.5575/geosoc.2015.0034 (in Japanese with English abstract)

Takahashi, S., Yamakita, S., Suzuki, N., Kaiho, K. and Ehiro, M. (2009) High organic carbon content and a decrease in radiolarians at the end of the Permian in a newly discovered continuous pelagic section: A coincidence? *Palaeogeography, Palaeoclimatology, Palaeoecology*, **271**, 1–12.

Takemura, A. (1986) Classification of Jurassic Nassellarians (Radiolaria). *Palaeontographica. Abteilung A: Palaozoologie-Stratigraphie*, **195**, 29–74.

Tan Sin Hok (1927) Over de samenstelling en het onstaan van krijt- en mergel-gesteenten van de Molukken. *Jaarboek van het mijnwezen in Nederlandsch Oost-Indie, jaargang 55, 1926, verhandelingen*, 3rd gedeelte, 5–165.

Tokiwa, T., Shimura, Y., Takeuchi, M., Shimosato, S., Yamamoto, K. and Mori, H. (2019) Provenance of trench-fill deposits of the Jurassic Chichibu accretionary complex, Southwest Japan. *Journal of Asian Earth Sciences*, **184**, 103970.

Toyohara, F., Uyesugi, K., Kimura, T., Ito, T., Murata, A. and Iwamatsu, A. (1980) Geosyncline in the northern Kitakami Massif and the Oshima Peninsula. *In*: Kimura, T. ed., Report on the Multidiscipline Reseach Project A with *1979 Foundation of Grant-in-Aid for Scientific Research by the Education Ministry of Japan*, Tokyo Print Insatsu, Ltd., Tokyo 27–36. (in Japanese)*

Uchino, T. (2017) Late Triassic U–Pb–zircon age from tuffaceous mudstone in the Kadoma Complex, North Kitakami Belt, Northeast Japan. *The Journal of the Geological Society of Japan*, **123**, 977–982.

Uchino, T. (2019) Detrital zircon U–Pb ages of sandstone within the Jurassic accretionary complex in the North Kitakami Belt of the Sotoyama District, Iwate Prefecture. *Bulletin of the Geological Survey of Japan*, **70**, 357–372. (in Japanese with English abstract)

Uchino, T. (2021) Middle Jurassic zircon age from

sandstone within the accretionary complex in the North Kitakami Belt, Kamatsuda area in Iwaizumi Town, Iwate Prefecture, Northeast Japan: Verifying the age of the accretionary complex containing the Okawa Sample. *Bulletin of the Geological Survey of Japan*, **72**, 99–107. (in Japanese with English abstract)

Uchino, T. and Suzuki, N. (2020) Late Jurassic radiolarians from mudstone near the U–Pb-dated sandstone of the North Kitakami Belt in the northeastern Shimokita Peninsula, Tohoku, Japan. *Bulletin of the Geological Survey of Japan*, **71**, 313–330. doi:10.9795/bullgsj.71.313

Ueda, H., Kimura, S., Saito, T., Takano, Y., Iizuka, N. and Orihashi, Y. (2018) Material recycling in a sediment-starved trench recorded in the Early Cretaceous Shiriya accretionary complex, Northeast Japan. *Island Arc*, **27**, 1–20. doi:10.1111/iar.12272

Wiedenbeck, M., Alle, P., Corfu, F., Griffin, W.L., Meier, M., Oberli, F., Quadt, A., Roddick, J.C. and Spiegel, W. (1995) Three natural zircon standards for U-Th-Pb, Lu-Hf, trace element and REE analyses. *Geostandards Newsletter*, **19**, 1–23.

Yamaguchi, Y. (1981) Geological structure of the eastern part of the North Kitakami Mountains, Japan—with special reference to structural subdivision. *Tohoku University, Institute of Geology and Paleontology Contributions*, **83**, 1–19. (in Japanese with English abstract)

Yamaguchi, Y., Tsushima, H. and Kitamura, N. (1979) Geologic development of the Southern part of 'Taro Belt' and 'Iwaizumi Belt' in the Kitakami Massif, Northeast Japan. *Tohoku University, Institute of Geology and Paleontology Contributions*, **80**, 99–117. (in Japanese with English abstract)

Yamakita, S. and Otoh, S. (2000) Cretaceous rearrangement processes of pre-Cretaceous geologic units of the Japanese Islands by MTL-Kurosegawa left-lateral strike-slip fault system. *The Memoirs of the Geological Society of Japan*, no. 56, 23–38. (in Japanese with English abstract)

Yamato Omine Research Group (1992) Mesozoic and Paleozoic Systems in the Central Area of the Kii Mountains, Southwest Japan (Part IV)—Mesozoic of the Takaharagawa District in Nara Prefecture—. *Earth Science (Chikyu Kagaku)*, **46**, 185–198. (in Japanese with English abstract)

Yamato Omine Research Group (2002) Mesozoic and Paleozoic Systems in the central area of the Kii Mountains, Southwest Japan (Part VII) —Mesozoic of the Shionoha area in Nara Prefecture—. *Earth Science (Chikyu Kagaku)*, **56**, 11–26. (in Japanese with English abstract)

Yamato Omine Research Group (2005) Mesozoic and Paleozoic Systems in the central area of the Kii Mountains, Southwest Japan (Part 9) —Reexamination of the Tsujido, Omine, Daiko and Kunimiyama areas—. *Earth Science (Chikyu Kagaku),* **59**, 287–300. (in Japanese with English abstract)

Yamato Omine Research Group (2007) Mesozoic and Paleozoic Systems in the central area of the Kii Mountains, Southwest Japan (Part 10)—The Mesozoic of the Osugi area in Mie Prefecture—. *Earth Science (Chikyu Kagaku)*, **61**, 33–47. (in Japanese with English abstract)

Yao, A. (1979) Radiolarian fauna from the Mino Belt in the northern part of the Inuyama Area, Central Japan, Part II: Nassellaria 1. *Journal of Geosciences, Osaka City University*, **22**, 21–72.

Yoshida, K. and Matsuoka, A. (2003) Pile-nappe structure of the Ryokami-yama chert unit in the Chichibu composite terrane of the Kanto Mountains, central Japan. *The Journal of the Geological Society of Japan*, **109**, 324–335. (in Japanese with English abstract)

Yoshida, T. and Katada, M. (1964) *Explanatory Text of the Geological Map of Japan, Scale 1: 50,000 'Otsuchi and Karodake' Akita, Nos. 35 and 36*. Geological Survey of Japan, Kawasaki, 30p.

Yoshida, T., Yoshii, M., Katada, M., Tanaka, K., Sakamoto, T. and Satoh, H. (1987) *Geology of the Rikuchu-Ono district*. With Geological Sheet Map at 1: 50,000. Geological Survey of Japan, Tsukuba, 70p.

*English translation from the original written in Japanese

Recieved March 18, 2022
Accepted October 4, 2022

Plate 1 Photomicrographs and SEM photographs of radiolarians obtained from Otr-NE-01 (Manganese nodule of the Okoshizawa Subunit).

1 *Japnocapsa fusiformis* (Yao)

2 *Gongylothorax siphonofer* Dumitrica

3 *Protunuma fusiformis* Ichikawa and Yao

4 *Striatojapnocapsa* sp.

5 *Diacanthocapsa*? *operculi* Yao

6 *Striatojaponocapsa synconexa* O'Dogherty, Goričan and Dumitrică

7 *Eucyrtidiellum unumaense* (Yao)

8 *Eucyrtidiellum unumaense* (Yao)

9 Multi-segmented nassellarian

10 *Pantanellium*? sp.

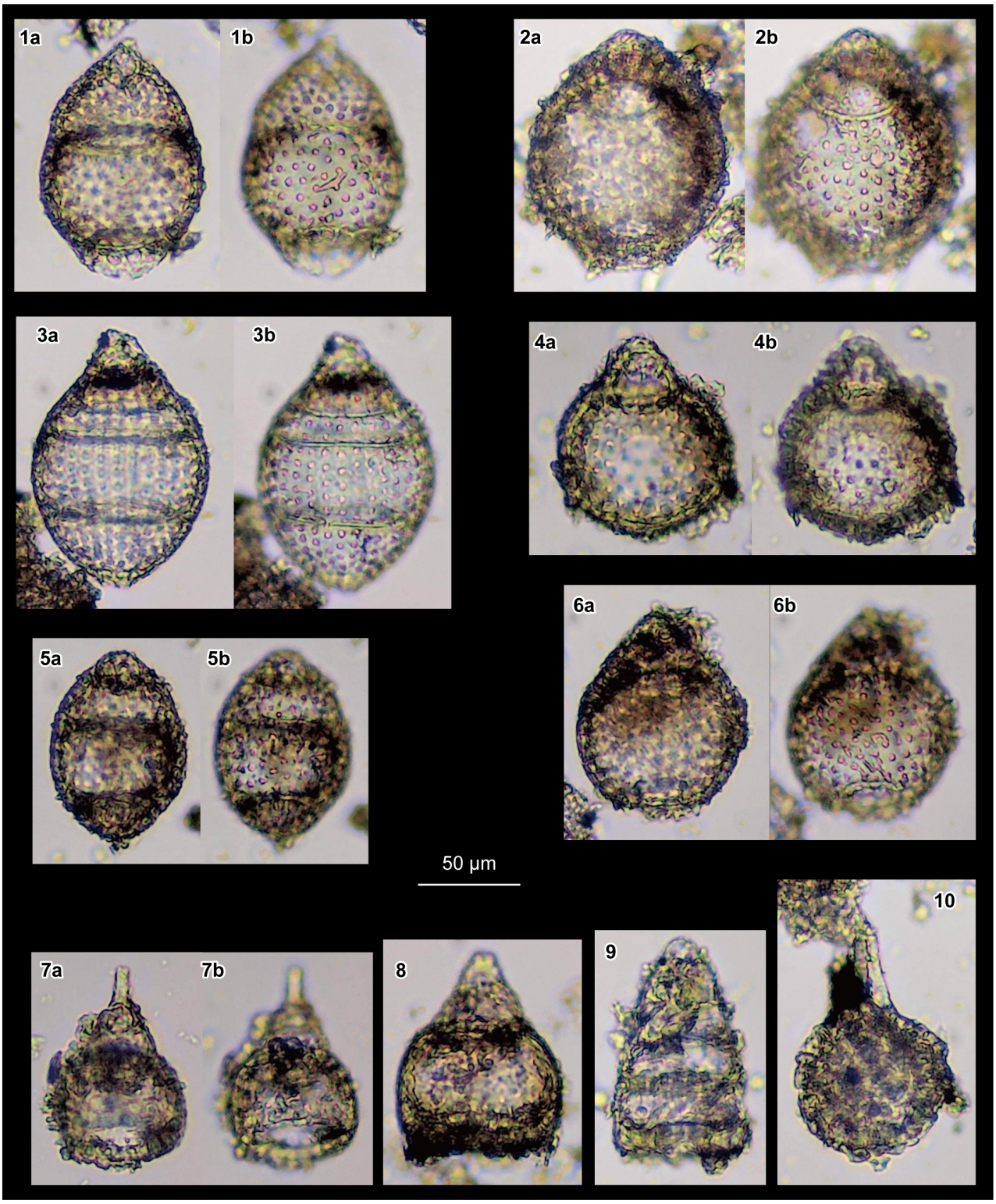
1a
1b
2a
2b
3a
3b
4a
4b
5a
5b
6a
6b
50 μm
7a
7b
8
9
10

Plate 2 Photomicrographs and SEM photographs of radiolarians obtained from Otr-N-02 (Siliceous mudstone of the Okoshizawa Subunit).

1 Closed nassellarian

2 Three-segmented closed nassellarian

3 Closed nassellarian

4 Williriedellidae gen. et sp. indet.

5 Williriedellidae gen. et sp. indet.

6 Closed nassellarian

7 Nassellaria gen. et sp. indet.

8 Nassellaria gen. et sp. indet.

9 Nassellaria gen. et sp. indet.

10 Multi-segmented nassellarian

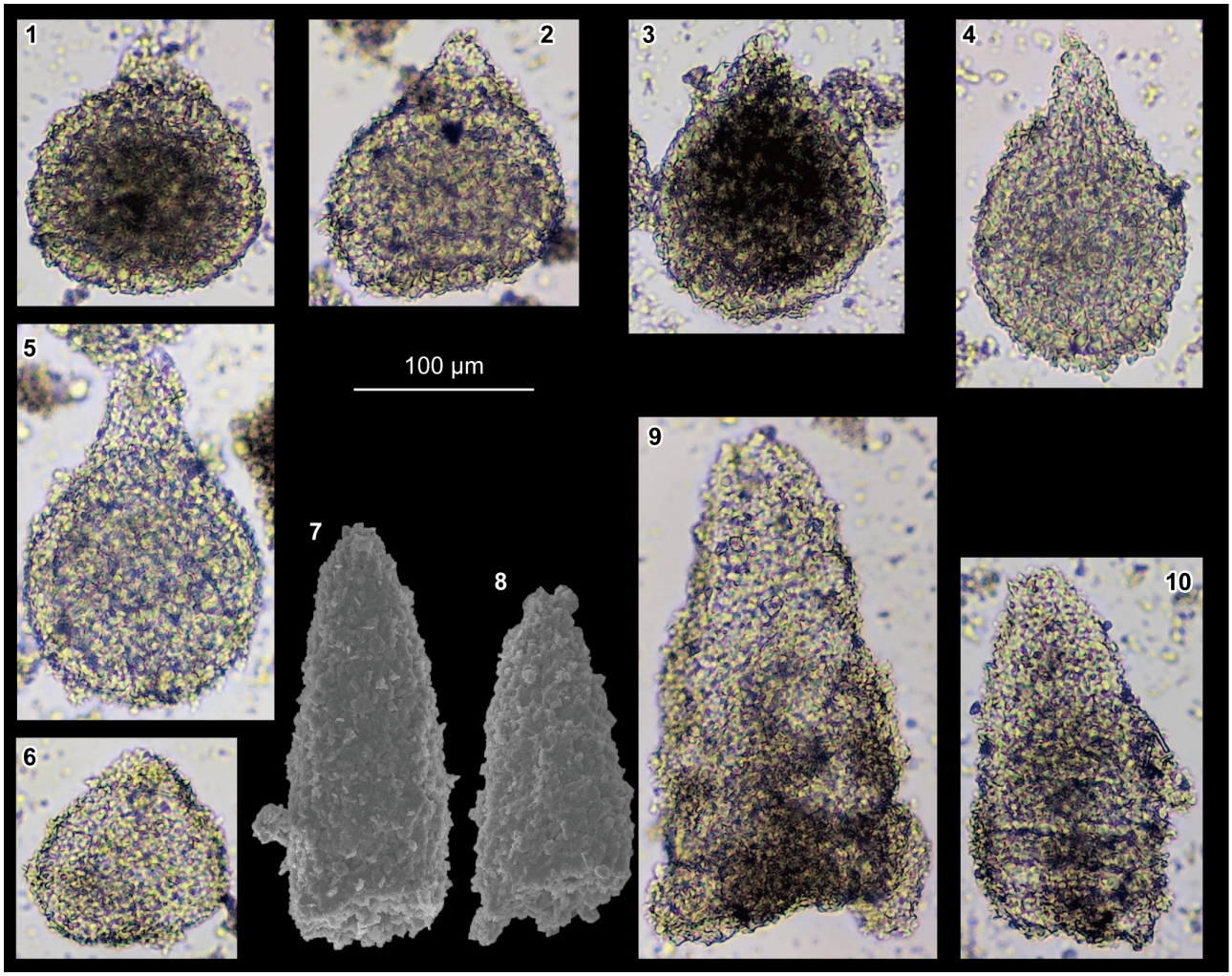
1
2
3
4
5
100 μm
9
7
8
10
6

Plate 3 Photomicrographs and SEM photographs of radiolarians obtained from Okz-15 (Siliceous mudstone of the Okoshizawa Subunit).

1 Williriedellidae gen. et sp. indet.

2 Williriedellidae gen. et sp. indet.

3 Closed nassellarian

4 Closed nassellarian

5 Closed nassellarian

6 Closed nassellarian

7 Closed nassellarian

8 Williriedellidae gen. et sp. indet.

9 Closed nassellarian

10 Closed nassellarian

11 Closed nassellarian

12 Closed nassellarian

13 Multi-segmented nassellarian

14 Nassellaria gen. et sp. indet.

15 Nassellaria gen. et sp. indet.

16 Spherical radiolarian

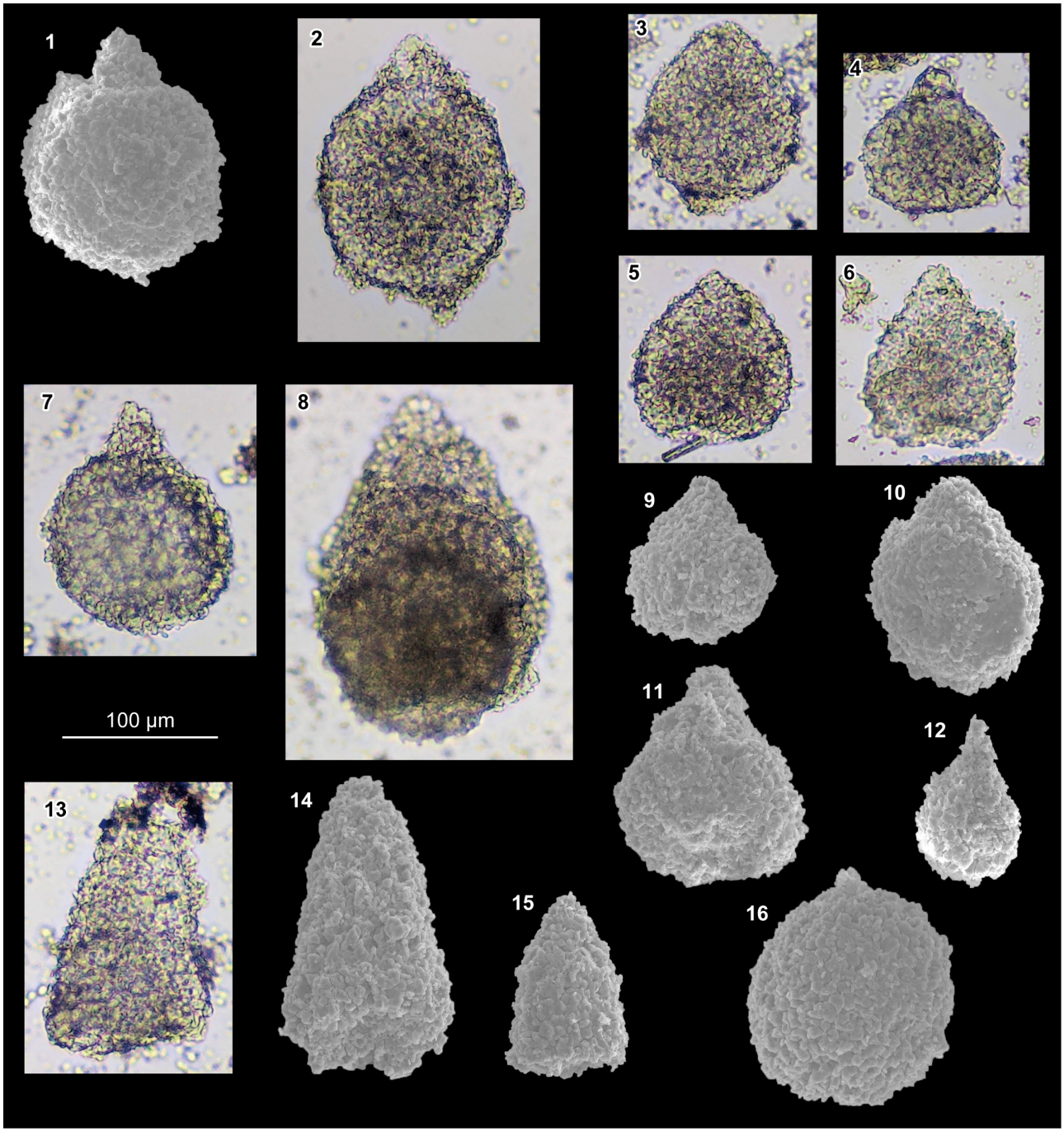
1
2
3
4
5
6
7
8
9
10
11
12
13
14
15
16
100 μm

Plate 4 Photomicrographs and SEM photographs of radiolarians obtained from Osm-12 (Siliceous mudstone of the Osakamoto Subunit).

1 *Striatojaponocapsa synconexa* O'Dogherty, Goričan and Dumitrică

2 Williriedellidae gen. et sp. indet.

3 Closed nassellarian

4 Closed nassellarian

5 Williriedellidae gen. et sp. indet.

6 Closed nassellarian

7 Closed nassellarian

8 Closed nassellarian

9 Closed nassellarian

10 *Eucyrtidiellum* sp.

11 *Eucyrtidiellum*? sp.

12 Nassellaria gen. et sp. indet.

13 Nassellaria gen. et sp. indet.

14 *Archaeodictyomitra* sp.

15 Nassellaria gen. et sp. indet.

16 *Charlottea*? sp.

17 *Hagistrum*? sp.

18 *Archaeospongoprunum*? sp.

19 *Archaeospongoprunum*? sp.

20 *Paronaella*? sp.

21 Eptingiidae gen. et sp. indet.

22 Spumellaria gen. et sp. indet.

23 Spumellaria gen. et sp. indet.

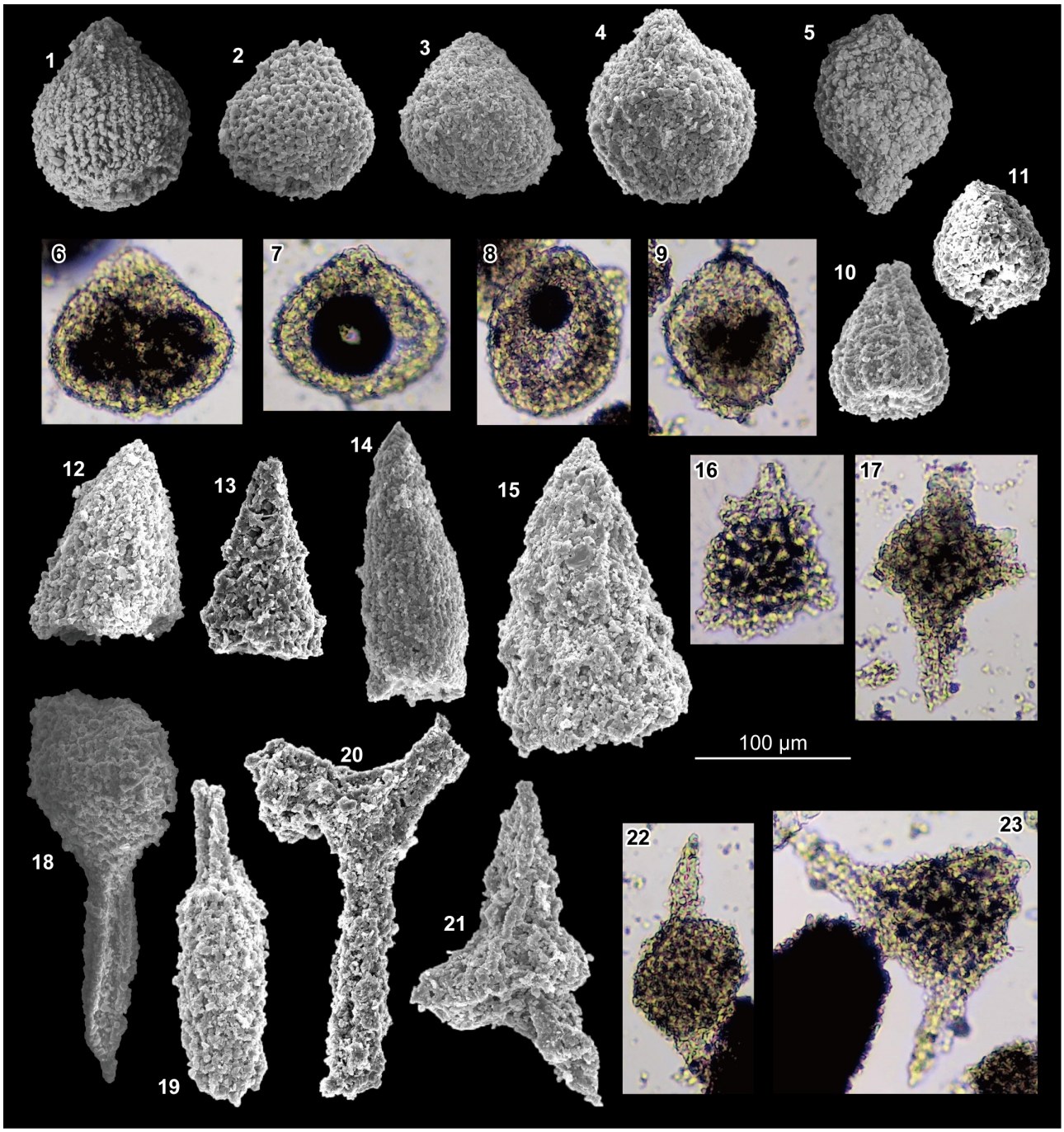
1
2
3
4
5
6
7
8
9
10
11
12
13
14
15
16
17
18
19
20
21
22
23
100 μm

Plate 5 Photomicrographs and SEM photographs of radiolarians obtained from Noz-02 (Siliceous mudstone of the Osakamoto Subunit).

1 *Japonocapsa* cf. *fusiformis* (Yao)

2 *Praezhamoidellum*? cf. *japonicum* (Yao)

3 Closed nassellarian

4 Closed nassellarian

5 Closed nassellarian

6 Closed nassellarian

7 Closed nassellarian

8 Closed nassellarian

9 Closed nassellarian

10 Nassellaria gen. et sp. indet.

11 *Hsuum* sp.

12 Multi-segmented nassellarian

13 Multi-segmented nassellarian

14 Multi-segmented nassellarian

15 Multi-segmented nassellarian

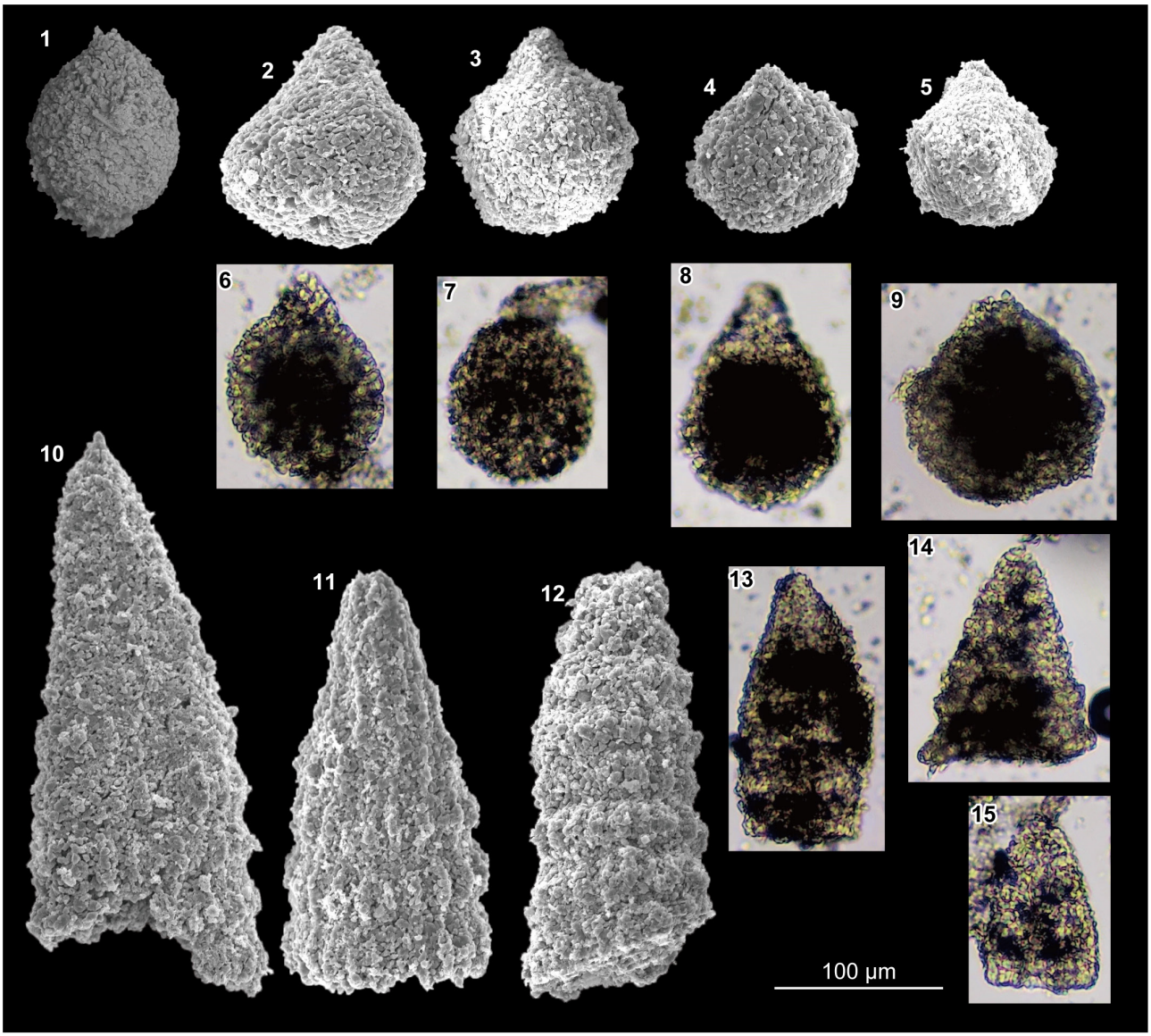
1
2
3
4
5
6
7
8
9
10
11
12
13
14
15
100 μm

Appendix

Table A1 Sample list.

Sample ID	Lithology	Locality		Subunit	Note
		°N	°E		
Okz-CO-01	Chert	40.007	141.606	Okoshizawa	Conodonts.
Otr-NE-01	Mn nodule	39.969	141.645	Okoshizawa	HCl treatment for radiolarians.
Otr-N-02	Siliceous mudstone	39.978	141.630	Okoshizawa	Dilute HF treatment for radiolarians.
Okz-15	Siliceous mudstone	39.992	141.606	Okoshizawa	Dilute HF treatment for radiolarians.
Noz-02	Siliceous mudstone	39.965	141.589	Osakamoto	Dilute HF treatment for radiolarians.
Osm-12	Siliceous mudstone	40.004	141.573	Osakamoto	Dilute HF treatment for radiolarians.
Wys-02*	Mn nodule	39.943	141.651	Osakamoto	HCl treatment for radiolarians.
Otr-01*	Mudstone	39.965	141.648	Osakamoto	Dilute HF treatment for radiolarians.
Okz-33	Sandstone	39.990	141.604	Osakamoto	Zircon U–Pb dating.
Skm-08	Sandstone	39.973	141.610	Osakamoto	Zircon U–Pb dating.

*no identifiable radiolarians were obtained.

Table A2 List of outcrops shown in the figures.

Figure	Geographic name	Locality		Subunit	Note
		°N	°E		
Figure 6A	Otori	39.966	141.638	Okoshizawa	Bedded chert
Figure 6B	Okoshi Stream	39.992	141.606	Okoshizawa	Siliceous mudstone
Figure 6C	Ananeyama Logging Road	39.962	141.651	Okoshizawa	Mudstone with broken sandstone
Figure 6D	Okoshi Stream	40.007	141.605	Okoshizawa	Dolostone and chert
Figure 6E	Otori	39.966	141.639	Okoshizawa	Green siliceous claystone
Figure 6F	Otori	39.966	141.639	Okoshizawa	Red siliceous claystone
Figure 6G	Orikabe	39.952	141.664	Okoshizawa	Chert, grey siliceous claystone, black carbonaceous claystone (Permian–Triassic Boundary)
Figure 6H	Okoshi Stream	40.006	141.605	Okoshizawa	Chert breccia
Figure 6I	Okoshi Stream	40.007	141.606	Okoshizawa	Chert breccia and mudstone
Figure 8A	Northeast of Otori	39.968	141.645	Okoshizawa	Siliceous mudstone with Mn nodule
Figure 9A	Okoshi Stream	39.987	141.602	Osakamoto	Mudstone
Figure 9B	Orikabe	39.947	141.663	Osakamoto	Mixed mudstone and sandstone
Figure 9C	Sakamoto	39.967	141.618	Osakamoto	Mixed rock
Figure 9D	Tengubatake Logging Road	39.943	141.650	Osakamoto	Bedded sandstone

Table A3 Occurrence list of radolarians.

Sample	Okoshizawa Subunit			Osakamoto Subunit	
	Otr-NE-01	Otr-N-02	Okz-15	Osm-12	Noz-02
	Mn nodule	si. md.	si. md.	si. md.	si. md.
Archaeodictyomitra sp.				x	
Diacanthocapsa? *operculi* Yao	x				
Eucyrtidiellum unumaense (Yao)	x				
Eucyrtidiellum sp.				x	
Eucyrtidiellum? sp.				x	
Gongylothorax siphonofer Dumitrica	x				
Hsuum sp.					x
Japnocapsa fusiformis (Yao)	x				
Japnocapsa cf. *fusiformis* (Yao)					x
Praezhamoidellum? cf. *japonicum* (Yao)					x
Protunuma fusiformis Ichikawa and Yao	x				
Striatojaponocapsa synconexa O'Dogherty, Goričan and Dumitrică	x			x	
Williriedellidae gen. et sp. indet.		x	x	x	
Nassellaria gen. et sp. indet.		x	x	x	x
Multi-segmented nassellarian	x	x	x		x
Three-segmented closed nassellarian		x			
Closed nassellarian		x	x	x	x
Archaeospongoprunum? sp.				x	
Charlottea? sp.				x	
Hagistrum? sp.				x	
Pantanellium? sp.	x				
Paronaella? sp.				x	
Eptingiidae gen. et sp. indet.				x	
Spumellaria gen. et sp. indet.				x	
Spherical radiolarian			x		

北部北上帯大鳥ユニットの地質と付加年代

武藤　俊・伊藤　剛・村山　雅史

要　旨

東北日本の北部北上帯に属するジュラ紀から白亜紀初期に形成された付加体は，同時代に形成された西南日本の付加体と比較して研究が少ない．本論文では，北部北上帯北東部，安家川上流に分布するジュラ紀付加体大鳥（おおとり）ユニットについての調査結果を報告する．詳細なマッピングに基づき，大鳥ユニットが，構造的下位を占めチャートと珪質泥岩の整然相が構造的に繰り返す大越沢サブユニットと，構造的上位を占め泥質岩に砂岩，チャート，微量の玄武岩類が含まれる混在相の大坂本（おおさかもと）サブユニットからなることを明らかにした．大越沢サブユニットの珪質泥岩中のマンガンノジュールから中期ジュラ紀バトニアン期を指示する放散虫化石が得られた．また，大坂本サブユニットの砂岩試料から抽出された砕屑性ジルコンは，約 170 Ma の最若年代を示す．放散虫および砕屑性ジルコンの年代から，大鳥ユニットの付加年代はバトニアン期と推定される．本研究のデータを用いて，北部北上帯と西南日本の南部秩父帯との対比について検討した．大鳥ユニットは構造的には南部秩父帯の大平山（おおひらやま）ユニットに対応し，両者は混在相からなる点で類似し，付加年代も重なっている．しかし，大鳥ユニットが石灰岩を欠く点と珪質泥岩の年代が若い点は大きな相違点であり，両者は厳密には対比できない可能性がある．

難読･重要地名

Kitakami 北上　Otori 大鳥　Akka 安家　Okoshizawa 大越沢　Osakamoto 大坂本　Kassenba 合戦場　Hiraniwadake 平庭岳